TURUN
YLIOPISTO
UNIVERSITY
OF TURKU

STUDIES ON DOSIMETRY OF POSITRON EMITTING RADIOPHARMACEUTICALS

Tuula Tolvanen

TURUN YLIOPISTON JULKAISUJA – ANNALES UNIVERSITATIS TURKUENSIS
SARJA – SER. D OSA – TOM. 1718 | MEDICA – ODONTOLOGICA | TURKU 2023

TURUN
YLIOPISTO
UNIVERSITY
OF TURKU

STUDIES ON DOSIMETRY OF POSITRON EMITTING RADIOPHARMACEUTICALS

Tuula Tolvanen

TURUN YLIOPISTON JULKAISUJA – ANNALES UNIVERSITATIS TURKUENSIS
SARJA – SER. D OSA – TOM. 1718 | MEDICA – ODONTOLOGICA | TURKU 2023

University of Turku

Faculty of Medicine
Medical Physics and Engineering
Doctoral Programme in Clinical Research
Turku PET Centre

Supervised by

Professor Mika Teräs
Department of Medical Physics
Turku University Hospital
Institute ot Biomedicine
University of Turku, Finland

Professor Heikki Minn
Department of Oncology
Turku University Hospital
Institute of Clinical Medicine
University of Turku, Finland

Reviewed by

Docent Eero Hippeläinen
Department of Clinical Physiology and Nuclear Medicine, University of Helsinki and Helsinki University Hospital, Helsinki, Finland

Docent Mattias Sandström
Department of Surgical Sciences, Radiology and Molecular Imaging, Uppsala University Hospital, Uppsala, Sweden

Opponent

Professor Mikko Tenhunen
HUS Comprehensive Cancer Centre, Radiation Therapy, Helsinki University Hospital, Helsinki, Finland

ISBN 978-951-29-9302-4 (PRINT)
ISBN 978-951-29-9303-1 (PDF)
ISSN 0355-9483 (Print)
ISSN 2343-3213 (Online)
Painosalama, Turku, Finland 2023

To my family

UNIVERSITY OF TURKU
Faculty of Medicine
Medical Physics and Engineering
Turku PET Centre
TUULA TOLVANEN: Studies on Dosimetry of Positron Emitting Radiopharmaceuticals
Doctoral Dissertation, 111 pp.
Doctoral Programme in Clinical Research
June 2023

ABSTRACT

Positron emission tomography (PET) is a non-invasive method for studying physiological phenomena in a living subject with radiopharmaceuticals. The physical decay of radioactive radiopharmaceuticals induce ionization in subjects, which results in an absorbed dose. Developing a new radiopharmaceutical always raises the question of how much of this substance can we inject into the patient? Administering radioactive substance to patients should always be justified and the potential benefit should outweigh the risk. Determining radiation doses for new positron emitting radiopharmaceuticals is an important part of the benefit-risk assessment of the use of radioactivity.

In this study, the evaluation of radiation doses was conducted using PET imaging technology. Prior to PET/CT scanners, studies were limited to dynamic imaging of just one part of the body (brain, thorax, abdomen or skeletal muscle). However, developments in the performance of PET scanners enabled producing series of whole body PET scans. With this whole body scanning method, more source organs were evaluated per participant and the number of measurements was increased per time-point with the same number of participants. This produced more precise temporal time-activity-curves for source organs and more precise radiation dose calculations.

Radiation doses were calculated using computer programs that are commonly used in published dosimetry studies. There were updates in the programs during the course of the study as mathematical models of the human anatomy became more sophisticated and coefficients reflecting the harm caused by radiation to tissues became more accurate.

Dosimetry is only one part in development of a new radiopharmaceutical, and based on the results in this thesis these radiopharmaceuticals can be introduced for clinical use from a radiation safety point of view.

KEYWORDS: [^{18}F]FETNIM, [^{11}C]MeAIB, [^{11}C]choline, [^{18}F]-rhPSMA-7.3, absorbed dose, equivalent dose, effective dose, positron emission tomography

TURUN YLIOPISTO
Lääketieteellinen tiedekunta
Lääketieteellinen fysiikka ja tekniikka
Valtakunnallinen PET keskus Turku
TUULA TOLVANEN: Tutkimuksia positroneja emittoivien radiolääkkeiden säteilyannoksista
Väitöskirja, 111 s.
Turun kliininen tohtoriohjelma
Kesäkuu 2023

TIIVISTELMÄ

Positroniemissiotomografia (PET) soveltuu hyvin erilaisten fysiologisten ilmiöiden kajoamattomaan kuvantamiseen elävässä kohteessa radiolääkkeiden avulla. Kun radiolääkkeen radioaktiivisuus hajoaa, syntyy ionisoivaa säteilyä, joka aiheuttaa kohteeseen säteilyrasitusta, absorboitunutta annosta. Uuden radiolääkkeen tuottamisen jälkeen herää kysymys, paljonko kyseistä radiolääkettä voi ihmiseen injektoida, jotta sen käyttö olisi oikeutettua ja radioaktiivisuuden käytöstä saatava hyöty olisi sen mahdollisesti aiheuttamaa haittaa suurempi. Säteilyannosten määrittäminen uusille positroneja emittoiville radiolääkkeille on tärkeä osa radioaktiivisuuden käytön hyöty-haitta arviointia.

Tässä tutkimuksessa säteilyannosten arviointiin käytettiin PET-kuvaustekniikkaa. Aluksi tutkimukset toteutettiin yhden kehon osan (aivot, rintakehä, vatsa tai reisilihakset) dynaamisella kuvaamisella, mutta PET-kameroiden suorituskyvyn kehityksen myötä otettiin käyttöön tutkittavan henkilön koko kehon PET kuvaussarja menetelmä. Tämän kehitysaskeleen johdosta voitiin mitata lukumääräisesti samasta koehenkilöiden joukosta useampia lähde-elimien mittausarvoja kussakin mittapisteessä ja laskettiin tarkempi arvio säteilyannoksesta.

Säteilyannokset laskettiin tietokoneohjelmilla, joita käytetään yleisesti tieteellisissä dosimetriajulkaisuissa. Ohjelmassa tapahtui kehitystä tutkimuksen aikana, koska ihmiskehon anatomian matemaattinen malli muuttui ja säteilyn kudoksille aiheuttamaa haittaa kuvastavat kertoimet tarkentuivat.

Säteilyannosten määrittäminen uudelle radiolääkkeelle on yksi osa radiolääkekehitystä. Tässä tutkimuksessa julkaistujen tulosten perusteella säteilyturvallisuuden näkökulmasta nämä radiolääkkeet voitiin ottaa kliiniseen käyttöön.

AVAINSANAT: [^{18}F]FETNIM, [^{11}C]MeAIB, [^{11}C]choline, [^{18}F]-rhPSMA-7.3, absorboitunut annos, ekvivalentti annos, efektiivinen annos, positroniemissiotomografia

Table of Contents

Abbreviations

[^{11}C]MeAIB	[*N*-methyl-^{11}C]α-methylaminoisobutyric acid
CT	Computed tomography based on Röntgen radiation
E	Effective Dose
EDE	Effective Dose Equivalent
E_i	Energy of the i^{th} transition
[^{18}F]FDG	2-deoxy-2-[^{18}F]-fluoro-D-glucose
[^{18}F]FETNIM	Fluoroerythronitroimidazole
[^{18}F]-rhPSMA	Radiohybrid prostate-specific membrane antigen
FBP	Filtered-back projection reconstruction algorithm
Gy	Gray, SI unit for absorbed dose
ICRP	International Commission of Radiation Protection
ICRU	International Commission of Radiation Units and Measurements
LET	Linear-energy-transfer
MIRD	Committee on Medical Internal Radiation Dose
MIRDOSE	First software code for calculate radiation doses
OLINDA	Software code for calculate radiation doses
PET	Positron Emission Tomography
RADAR	Radiation Dose Assessment Resource
RBE	Relative Biological Effectiveness
ROI	Region of interest
SI	International System of Units
SNM	Society of Nuclear Medicine
Sv	Sievert, SI unit for equivalent and effective doses
TAC	Time Activity Curve
VOI	Volume of Interest
WMA	World Medical Association
w_R	Radiation weighting factor defined by regulation
w_T	Tissue weighting factor defined by regulation

List of Original Publications

This dissertation is based on the following original publications, which are referred to in the text by their Roman numerals:

I Tolvanen T, Lehtiö K, Kulmala J, Oikonen V, Eskola O, Bergman J, Minn H. [^{18}F]Fluoroerythronitroimidazole radiation dosimetry in cancer studies. *J Nucl Med*, 2002; 43: 1674-80.

II Tolvanen T, Någren K, Yu M, Sutinen E, Havu-Aurén K, Jyrkkiö S, Asola M, Kotoneva E, Nuutila P, Minn H. Human radiation dosimetry of [^{11}C]MeAIB, a new tracer for imaging of system A amino acid transport. *Eur J Nucl Med Mol Imaging*, 2006; 33: 1178-84.

III Tolvanen T, Yli-Kerttula T, Ujula T, Autio A, Lehikoinen P, Minn H, Roivainen A. Biodistribution and radiation dosimetry of [^{11}C]choline: a comparison between rat and human data. *Eur J Nucl Med Mol Imaging,* 2010; 37: 874-83.

IV Tolvanen T, Kalliokoski K, Malaspina S, Kuisma A, Lahdenpohja S, Postema EJ, Miller MP, Scheinin M. Safety, biodistribution and radiation dosimetry of [^{18}F]-rhPSMA-7.3 in healthy adult volunteers. *J Nuc Med*, 2020; 62(5), 679–684.

1 Introduction

Positron emission tomography (PET) is a non-invasive method for imaging physiology in a living body. The signal for tomographic PET images originates from radioactive nuclides of radiopharmaceuticals, which are injected into the study subject. Radiopharmaceuticals include positron emitting nuclei (for example [^{11}C], [^{15}O], [^{18}F] or [^{68}Ga]) and radiation interacts with living tissue after intravenous injection. The disintegration of the unstable nuclei emits a positron ranging a few millimeters and interacting with the material inside the body. After losing its energy the positron annihilates with a rest state electron. This annihilation generates two annihilation photons travelling in opposite directions. The PET scanner collects these photons with coincidence timing technique and reconstructs the PET image.

The positron range inside the body is dependent on the positron's energy. The main interaction between the positron and the living tissue is inelastic scattering. It is the main cause of the internal absorbed dose. The annihilation gamma photons ionize tissue molecules through Compton scattering. Both interactions in the body may cause biological effects. For biological risks estimation, it is important to calculate the radiation exposure caused by a radiopharmaceutical in PET.

Before it is ethically acceptable to use novel radiopharmaceuticals for human studies, toxicity, safety and tolerability must be guaranteed with preclinical research. In the beginning the calculations of radiation burden caused by the novel radiopharmaceutical are based on preclinical research or prior information of similarly behaving radiopharmaceuticals. In Turku PET Centre the procedure with the novel radiopharmaceutical includes PET imaging and radiation dose calculation from at least six volunteers before it can be further used in clinical or scientific PET studies. In this thesis the biodistribution, radiation doses and radiation safety of four different radiopharmaceuticals were studied. Development in the methods of collecting the biodistribution data is described as imaging technology has improved over the years. All radiopharmaceuticals were synthetized in Turku PET Centre radiochemistry laboratory. PET or PET/CT scanners in Turku PET Centre acquired the biodistribution of [^{18}F]FETNIM, [^{11}C]MeAIB, [^{11}C]choline and [^{18}F]-rhPSMA-7.3.

2 Review of the Literature

2.1 Dosimetry

Dosimetry is a process or method for measuring the dosage of ionizing radiation. The term ionizing radiation is used to describe the transfer of energy through space in the form of either electromagnetic waves or subatomic particles that are capable of causing ionization in matter.

Ionization is the process by which atoms lose or gain electrons. Those atoms become ions, electrically charged atoms, kations or anions (ICRP, 1991a). In ions, the amount of protons in nuclei and the number of electrons in its orbit is not equal.

Dosimetry is used for radiation protection or for the optimization of radiation utilization. The aim of dosimetry is to give estimates of absorbed radiation doses in a living subject. Dosimetry includes internal or external dosimetry for radiation workers, the general public and subjects exposed to radiation during medical use of radiation. External medical exposure dosimetry is based on measurements with dosimeters. Internal dosimetry relies on a variety of monitoring, bio-assay or radiation imaging techniques in determining radiation doses. Another term for dosimetry is dose assessment (<*https://Doseinfo-Radar.Com*>).

The biological risk estimates caused by ionizing radiation are connected to dosimetric calculations. The administered activity, the dose rate and the quality of the radiation influence the effect of ionizing radiation (ICRP, 1981). In internal exposure and in nuclear medicine imaging, the absorbed dose is influenced by the amount and biokinetics of the administered radiopharmaceutical and the physical characteristics of the radionuclide in radiopharmaceutical (ICRP, 1987a). For biological risk estimation the sensitivity to radiation induced harm in different organs must be included in calculations (ICRP, 1991a).

2.2 Committees for medical internal dosimetry

In internal dosimetry the radiation source is inside the subject and doses can not be measured directly. For this purpose radiation protection committees have developed standardized methods. The internal dosimetry schema of the Medical Internal Radiation Dose (MIRD) Committee of the Society of Nuclear Medicine has given a

comprehensive framework for the assessment of the radiation doses (Bolch et al., 2009). Prior to the MIRD committee, scientists interested in nuclear medicine had meetings in the 1950s and they published the first schema of internal dosimetry in 1968 as a MIRD Pamphlet No. 1 (Howell et al., 1999). The Committee continues to develope standardized methods, models and mathematical schema for estimating internal radiation doses from administered radiopharmaceuticals (Society of Nuclear Medicine and Molecular Imaging). Nowadays estimated absorbed doses have been reported for whole organs, tissue subregions, voxelized tissue structures, and individual cellular compartments for use in both diagnostic and therapeutic nuclear medicine (Bolch et al., 2009). New methods are published as series in the Journal of Nuclear Medicine (J Nucl Med), called MIRD Pamphlet. Also, radiation absorbed doses from radiopharmaceuticals have been published in MIRD Dose Estimate Report-series in J Nucl Med. These reports consists mostly of traditional nuclear medicine radiopharmaceuticals labelled with [^{99m}Tc].

The International Commission on Radiological Protection (ICRP) was originally established to give radiation protection guidance for radiation workers and the general public. ICRP is an independent commission, that publishes radiation protection recommendations based on scientific evidence (<*https://WWW.ICRP.Org*>). It was established in 1928 and it still gives new recommendations for protection against harmful effects of ionizing radiation when new scientific knowledge appears. Recommendations are published as Annals of the ICRP Publication. Nowadays ICRP has developed a dosimetry schema for internal dosimetry similar to that of the MIRD Committee. These two committees use different terminology and symbols for fundamental quantities, such as the absorbed fraction, specific absorbed fraction, and various dose coefficients (Bolch et al., 2009).

The two systems for calculating doses in internal dosimetry are, the ICRP 30/60 system and the MIRD system. ICRP publishes radiation dose estimates for diagnostic radiopharmaceuticals, which are in general use. In 1987, ICRP Publication 53 (ICRP, 1987b) published dose coefficients for 120 radiopharmaceuticals. In 1991, dose data for six additional radiopharmaceuticals were published in ICRP Publication 62, which includes Addendum 1 to ICRP Publication 53 (ICRP, 1991b). Data for another 10 radiopharmaceuticals were published in ICRP Publication 80, which superseded Addentum 1 and is Addentum 2 to ICRP Publication 53 (ICRP, 1998). A third Addendum to ICRP Publication 53, the biokinetic information and dose coefficients covering 25 different radiopharmaceuticals was published in ICRP Publication 106 (ICRP, 2008). A fourth Addentum to ICRP Publication 53 including 6 radiopharmaceuticals, was published in 2013; Radiation dose to patients from radiopharmaceuticals. It has been available on the ICRP's website, www.icrp.org. At the time of writing this thesis the latest ICRP publication for radiopharmaceuticals is ICRP Publication 128 Radiation Dose

to Patients from Radiopharmaceuticals: A Compendium of Current Information Related to Frequently Used Substances, 2015 (ICRP, 2015).

The International Commission on Radiation Units and Measurements (ICRU) has also published information regarding dose calculations from radiopharmaceuticals. ICRU Report 32 in 1979 is Methods of Assessment of Absorbed Dose in Clinical Use of Radionuclides and ICRU Report 67 in 2002 is Absorbed-dose specification in nuclear medicine (ICRP, 2015)(Johansson et al., 1992). The principal objective for the ICRU has been the development of internationally acceptable recommendations regarding quantities and units of radiation and radioactivity. The procedures suitable for the measurement and applications of these quantities in clinical radiology and radiobiology, and the physical data needed in the application of these procedures - the use of which tends to assure uniformity in reporting - are also targets for the ICRU. The ICRU makes similar types of recommendations for the radiation protection field in close cooperation with the ICRP (Wambersie, 2002). Beginning in 2019, ICRU reports have been published as the Journal of the ICRU.

The Radiation Dose Assessment Resource (RADAR) is the web site to bring radiation dosimetry to the 21st century. The goal of RADAR is to bring together various resources that exist in the areas of internal or external dosimetry, or as they say: internal or external dose assessment. In internal dose assessment, RADAR has mostly had impact on modernization of human anatomical models, phantoms. The original stylized dosimetry phantoms of the 1980s and the 1990s were a collection of spheres and cylinders in the shape of a robust human. Now RADAR has introduced the phantom as image-based voxelized models (<*https://Doseinfo-Radar.Com*>).

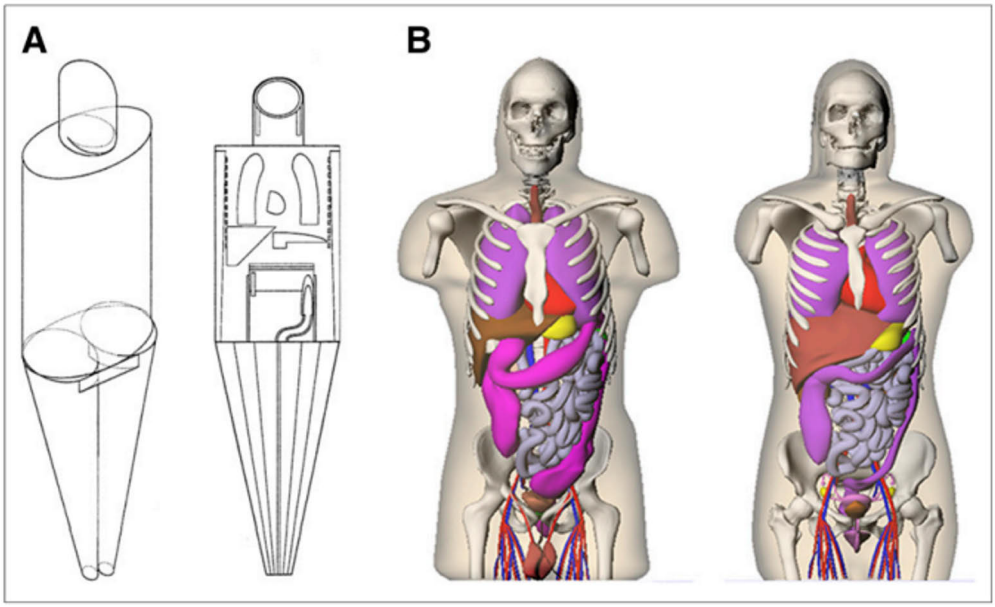

Figure 1. (A) Cristy-Eckerman stylished computational phantoms and (B) realistic voxel-based phantoms. This Figure was originally published in JNM Michael G. Stabin and Jeffry A. Siegel, RADAR Dose Estimate Report: A Compendium of Radiopharmaceutical Dose Estimates Based on OLINDA/EXM Version 2.0 2018;59:154-160. ©SNMMI.

2.3 Basic dosimetric quantities

2.3.1 Radioactivity

Radioactivity is the number of spontaneous disintegrations of unstable atomic nuclei per second, s^{-1}. The International System of units (SI) defines this unit as becquerel (Bq). At the time Marie Curie discovered radioactivity in 1898 the unit of radioactivity was curie (Ci). It was defined as disintegrations of 1 gram of pure radium-226 isotope. The relation between these two units is 1 mCi = 37 MBq.

2.3.2 Absorbed dose

Absorbed dose, D, for a material is the absorbed energy per unit mass, joule per kilogram (J/kg). The derived SI unit for absorbed dose is gray (Gy). Absorbed dose is used as the absolute dose value in organ or tissue, for example, in radiotherapy or in interventional radiology. It is defined as the dose specified at a point, but for nuclear medicine point of view absorbed dose means average dose over tissue or organ. The former unit for absorbed dose was rad and the relation between these two units is 100 rad = 1 Gy. Absorbed dose is defined as:

$$D = \frac{d\varepsilon}{dm} \quad \text{(Eq 1)}$$

where dε is the mean energy imparted by ionizing radiation to matter of mass dm.

2.3.2.1 Absorbed dose in internal dosimetry

Absorbed dose in internal dosimetry is defined as:

$$D = \frac{k\,\tilde{A}\sum_i n_i E_i \phi_i}{m} \quad \text{(Eq 2)}$$

where D= absorbed dose (Gy)
k= proportionality constant (Gy-kg/MBq-sec-MeV)
Ã= cumulated activity (MBq-sec)
n_i= number of radiations with energy E emitted per nuclear transition
E_i= energy for the radiation emitted by the nuclide (MeV)
ϕ_i= fraction of energy absorbed in the target
m= mass of target region (kg).

2.3.2.2 The Medical Internal Radiation Dose (MIRD) system

The MIRD schema simplifies the complexity of assessing absorbed dose for different radionuclides. The biological environments in which dose assessment can be done are the human body, internal organs, tissues, fluid compartments or cells. The MIRD schema systematically reduces complex dosimetric analyses to methods that are relatively simple for users, including software tools for experimental and clinical use.
The equation for absorbed dose in the MIRD system by Loevinger et al. 1988 (Loevinger et al., 1988) is simple:

$$D = \tilde{A}S \quad \text{(Eq 3)}$$

The cumulated activity Ã is another factor and all other terms are combined in the factor S:

$$S = \frac{k\,\sum_i n_i E_i \phi_i}{m} \quad \text{(Eq 4)}$$

S-values for a reference person model include reference person anatomic models, characteristics of radionuclide (half-life, emission types and energies, decay products and penetration ability of the radiation) and the specific fraction of absorbed energy to each source - target organ pair.

Absorbed fraction, ϕ, is the fraction of the energy emitted by the source and deposited in the target. Absorbed fraction depends on the type and energy of the

radiation, the size, shape and composition of the source and target, and the distance between the source and the target as well as the type of material separating them. For photons (gamma and x-rays) some of the emitted energy will escape objects that are of the the size and composition of interest to internal dosimetry. Absorbed fractions for electrons and beta particles are generally held to be 1.0 for an organ irradiating itself and 0.0 for any organ irradiating another organ (<*https://Doseinfo-Radar.Com*>). The Monte Carlo method, which is numerical modelling system based on probability and statistics, is utilized in the calculation of absorbed fractions for source organs irradiating themselves and other organs.

S-values are tabulated as source organ - target organ pairs for selected radionuclides. Anatomic models, phantoms, are used to mimic the human body, including different ages and sexes, during S-value calculations for modelling organ volumes and distances from other organs. These phantoms have developed over the course of decades from robust set of cylinders to image derived pixelized phantoms as shown in Figure 1.

2.3.2.3 Absorbed dose in this study

For the absorbed dose, D, calculations of all physical characteristics of the radionuclide and selected anatomic model are included in the S-value. The task in this research is to define the cumulated activity Ã in source organs. Cumulated activity in a source organ is estimated using biodistribution measurements. This is done through preclinical *ex vivo* measurements or dynamic PET imaging. The spatial and temporal variation of source organ radioactivity must be evaluated. The biokinetics of the radiopharmaceutical in each source organ is expressed as a function of time. When organ specific time-activity curves are generated, the cumulated activity in each organ can be estimated from the area under the curve.

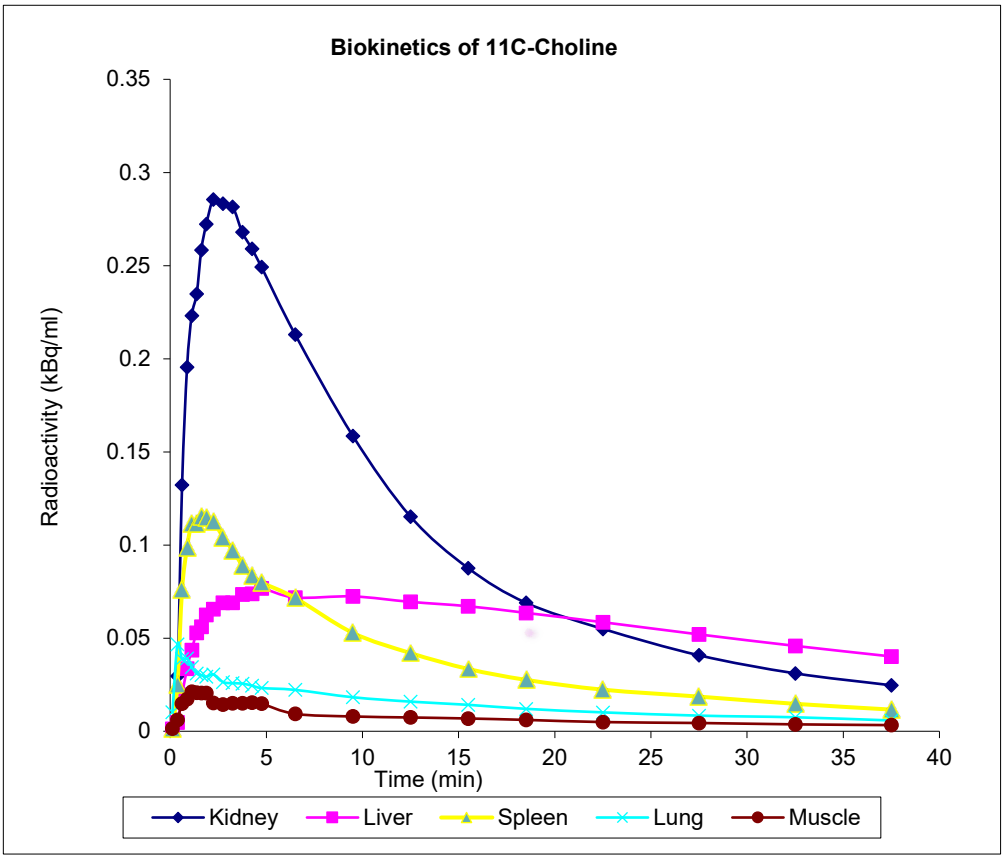

Figure 2. An example of time activity curves from dynamic imaging with PET. Data for this figure is from Study III in this thesis modified by author Tuula Tolvanen.

2.3.3 Equivalent dose

From a radiation protection point of view the absorbed dose averaged over a tissue or organ weighed for the radiation quality factor is of interest. For this purpose the term equivalent dose was introduced by the ICRP in Publication 30 (ICRP, 1979). The radiation weighting factor, w_R, expresses relative biological effects from a particular type of radiation in inducing stochastic effects at low doses. The factor is selected for the type and energy of the radiation emitted by the source (ICRP, 1991a).

The equivalent dose, H_T, in tissue T is given by the equation

$$H_T = \sum_R w_R \cdot D_{T,R} \qquad \text{(Eq 5)}$$

where $D_{T,R}$ is the absorbed dose average over the tissue or organ, T, due to radiation, R, and w_R is the radiation quality factor. The unit of the equivalent dose is joule per kilogram with the special name sievert (Sv).

The previous quantity for the product of the absorbed dose and the radiation quality factor before ICRP Publication 30 in 1979 was the dose equivalent. It was defined as the absorbed dose at a point multiplied by the radiation quality factor Q. The Q of a radiation type is defined as the ratio of the biological damage produced by the absorption of 1 Gy of that radiation to the biological damage produced by the same absorbed dose of x-rays or gamma rays (ICRP, 2003). Q values were 1 for photons and electrons, 5 for thermal neutrons and 20 for fast neutrons and alpha particles.

Now the ICRP has published updated weighting factors, w_R, in ICRP Publication 30, year 1979, ICRP Publication 60, year 1991 and in ICRP Publication 103, year 2007. As knowledge in biology and dosimetry has improved over years, the radiation weighting factors, w_R, have become more precise. The weighting factor of neutrons especially has changed to a continuous formula.

Table 1. Radiation weighting factors*.

Type and energy range	w_R ICRP 30, 1979	w_R ICRP 60, 1991
Photons, all energies	1	1
Electrons and muons, all energies**	1	1
Neutrons, energy < 10 keV	-	5
10 keV to 100 keV	-	10
> 100 keV to 2 MeV	-	20
> 2 MeV to 20 MeV	-	10
> 20 Mev	-	5
Protons, other than recoil protons, energy > 2MeV	-	2 – 5
Alpha particles, fission fragments, heavy nuclei	20	20

* All values related to the radiation incident on the body or, for internal sources, emitted from the source.

** Excluding Auger electrons emitted from nuclei bound to DNA.

Table 2. Radiation weighting factors* continues.

Type and energy range	ICRP 103, 2007
x-rays, gamma rays, beta particles, muons	1
Neutrons, energy < 1 MeV	$2.5 + 18.2\ e^{-[\ln(E)*\ln(E)]/6}$
1 MeV to 50 MeV	$5.0 + 17.0\ e^{-[\ln(2E)*\ln(2E)]/6}$
> 50 Mev	$2.5 + 3.25\ e^{-[\ln(0.04E)*\ln(0.04E]/6}$
Protons, changed pions	2
Alpha particles, nuclear fission products, heavy nuclei	20

* All values related to the radiation incident on the body or, for internal sources, emitted from the source.

2.3.4 Effective dose

The ICRP has provided the term effective dose, E, for estimating the whole body radiation dose and for comparing radiation doses from different exposures. Effective dose is the sum of equivalent doses multiplied by the tissue weighting factors. The equivalent dose, H_T, should only be used as a quantity for calculating the effective dose.

$$E = \sum_T w_T \cdot H_T \qquad \text{(Eq 6)}$$

The specific normalised values of tissue weighting factors w_T are defined by ICRP for individual tissues. Factors are used as an approximate age- and sex-averaged representation of the relative contribution of each tissue to the radiation detriment of stochastic effects from whole-body low linear-energy-transfer (LET) irradiations.

The values of both radiation and tissue weighting factors are informed by current knowledge of biophysics and radiobiology. The ICRP published tissue weighting factors in ICRP Publication 26, year 1977, ICRP Publication 60, year 1991 and in ICRP Publication 103, year 2007.

Table 3. Tissue weighting factors recommended by the ICRP Commission for stochastic risks.

Tissue	w_T ICRP 26, 1977	w_T ICRP 60, 1991	w_T ICRP 103, 2007
Gonads	0.25	0.20	0.08
Breast	0.15	0.05	0.12
Bed bone marrow	0.12	0.12	0.12
Colon	-	0.12	0.12
Stomach	-	0.12	0.12
Lung	0.12	0.12	0.12
Liver	-	0.05	0.04
Thyroid	0.03	0.05	0.04
Oesophagus		0.05	0.04
Bladder	-	0.05	0.04
Bone surfaces	0.03	0.01	0.01
Skin	-	0.01	0.01
Brain	-	-	0.01
Salivary glands	-	-	0.01
Remainder ICRP 26 and ICRP 60	0.30*	0.05**	
Remainder tissues***	-	-	0.12
Total, sum of w_T values	-	-	1.0

*The weighting factor for the remainder in the effective dose equivalent is to be divided equally among the five highest organs not explicitly mentioned in the list which receive the highest absorbed doses.

** The weighting factor for the remainder in the effective dose is to be divided equally among the organs not explicitly mentioned in this list but which were assigned by the ICRP (adrenals, brain, ULI, small intestine, kidneys, muscle, pancreas, spleen, thymus and uterus).

***Remainder tissues: Adrenals, extrathoracic (ET) region, gall bladder, heart, kidneys, lymphatic nodes, muscle, oral mucosa, pancreas, prostate, small intestine, spleen, thymus, uterus/cervix.

The effective dose is meant to present the equivalent dose in the condition that if received uniformly by the whole body it would result in the same total risk as that actually caused by a given nonuniform irradiation (Stabin, 2017). The effective dose can, for example, be used to compare different procedures, protocols and modalities for planning and optimizing radiation protection. It is a central dose quantity for regulatory purposes. E is not recommended to provide estimates of risk to individual patients, since it is based on sex- and age-averaged reference human dimensions.

Both equivalent and effective dose provide a basis for estimating the probability of stochastic effects only for absorbed doses well below the thresholds for deterministic effects.

Effective dose equivalent, EDE, was the previous whole body dose defined by the ICRP in 1979. EDE or H_e was the sum of dose equivalents and tissue weighting factor product, and it deviates from effective dose, E, by different weighting factors.

2.4 Dose calculation software

The MIRD schema from the Committee of the Society of Nuclear Medicine was developed to calculate the absorbed dose for whole organs in both diagnostic and therapeutic nuclear medicine. The schema was originally published in 1968, revised in 1976 and republished in 1988 and 1991 as the book MIRD Primer for Absorbed Dose Calculations (Bolch et al., 2009). The equation to the mean absorbed dose (D) in a target organ (r_k), from injected activity (A_0) is:

$$\frac{\overline{D}(r_k)}{A_0} = \sum_h \tau_h S(r_k \leftarrow r_h) \qquad \text{(Eq 7)}$$

where the S value contains physical characteristics of radionuclide (half-life, emission types and energies, decay products and penetration ability of the radiation) and the specific fraction of absorbed energy to each source-target organ pair (Howell et al., 1999). Residence time (τ_h) includes the kinetics of the radionuclide in the source organ (r_h). It can be called as time-integral activity coefficient since it is defined as the fraction of cumulated activity in the source organ and administered activity. It should not be confused with the mean lifetime of the radioactivity in the source region. Unlike the mean lifetime, the residence time also covers the uptake of radioactivity in the source region relative to the injected activity.

A computer software code called ‘MIRDOSE’ was developed to facilitate automated and standardised internal dose calculations for nuclear medicine applications by Michael Stabin in 1996 (Stabin, 1996). This code was completely rewritten and renamed to ’OLINDA/EXM’ (Organ Level INternal Dose Assessment/Exponential Modelling) in 2004. Even if the software name MIRDOSE can easily be connected to MIRD Committee, the software is not endorsed by the MIRD Committee of the Society of Nuclear Medicine (Stabin, 1996). The next generation of internal dose assessment software is named therefore OLINDA/EXM.

The code uses the same technical basis (phantoms, organ masses, equations, relationships assumed and other details) and radionuclides (used with nuclear medicine imaging with gamma cameras and positron emission tomography and therapy) as the MIRDOSE code and RADAR system (ICRP, 2015).

Just like with the MIRDOSE, users will enter results of biokinetic measurements into the OLINDA/EXM code, which uses them with models of the human body, to calculate estimates of the radiation dose to certain target organs and the body. The dose factors used in OLINDA/EXM are those found on the RADAR page on model dose factors. The OLINDA/EXM software has the United States Food and Drug Administration's (FDA) approval (Stabin et al., 2005).

The physical models, phantoms, that the code uses are stylized approximations of the human body based on idealized average individuals. It includes models of the adult male, adult female, children of various ages and females at different stages of pregnancy. The code provides estimates of the radiation dose per unit administered activity based on user entered source organ residence times for a given radionuclide and the selected human phantom.

2.5 Positron emission tomography

Positron emission tomography (PET) is a non-invasive imaging method that uses small amounts of radioactive material called radiopharmaceuticals, a special PET, PET/CT or PET/MR scanner and a computer system to reconstruct and archive 3-dimensional images of living objects. PET images illustrate quantitative changes at the cellular level and display tissue functionality or physiological processes.

Radiopharmaceuticals play an important role in PET imaging. They are molecules labelled with radioactive isotopes, radionuclides, like [^{11}C] or [^{18}F]. These radionuclides are unstable isotopes which decay spontaneously through β^+, positron emission to a more stable atomic state. Positron decay is characterized by the following decay equation.

$$p \rightarrow n + \beta^+ + \nu \qquad \text{(Eq 8)}$$

where p is a proton of a parent nucleus, n is a neutron of a daughter nucleus, β^+ is a positron, and ν is a neutrino, a particle with unknown very small mass or charge. The neutrino always accompanies the positron in the decay process due to the law of conservation in particle physics. Positron emission occurs in nuclei that are unstable because there is an excess number of protons compared to the number of neutrons in the nuclei. Positron decay is more prevalent in nuclei with low atomic numbers and can occur when the energy states of the parent and daughter differ by more than 1.022 MeV. The energies of the positron and neutrino are variable but constrained so that their total energy is equal to the difference in energy states of parent and daughter minus 1.022 MeV. Thus the positron energy varies from zero to its maximum value (Patton, 2002).

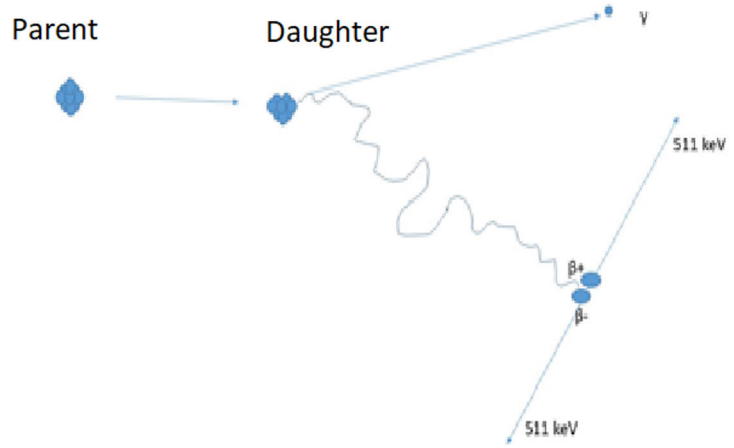

Figure 3. Positron emission and annihilation, figure modified by the author Tuula Tolvanen.

When a positron emits from the nucleus it has a characteristic range to travel before annihilation with an electron. Annihilation is the process that occurs when a particle collides with its respective antiparticle to produce other particles. In this case a positron collides with an electron to produce two annihilation photons with 511 keV energy on each. The annihilation photons are very energetic (they fall in the gamma ray region of the electromagnetic spectrum and are roughly a factor of ten higher in energy than diagnostic x-rays), which means that they have a good chance of escaping the body for external detection. Half value layer for 511 keV photons in water or in body is 7 cm. In a typical PET scan, many millions of these annihilation photon pairs will be detected from the injected radiopharmaceutical (Cherry & Dahlbom, 2004).

Physical characteristics for [^{11}C], [^{15}O], [^{18}F], [^{64}Cu] and [^{68}Ga] are given in Table 4.

Table 4. Physical characteristics of radionuclides (Patton, 2002).

Positron emitter	Half-life (min)	Daughter	β^+ %	Maximum energy (MeV)	Mean range (mm)
Carbon - 11	20.4	Boron - 11	100	0.96	0.3
Oxygen - 15	2.05	Nitrogen-15	100	1.72	1.5
Fluorine - 18	109.8	Oxygen - 18	97	0.64	0.2
Copper - 64	762	Nickel - 64	18	0.65	0.2
Gallium - 68	68	Zinc - 68	88	1.89	1.9

The spontaneous decay for all positron emitters is not purely emission of positrons from the nucleus. The percentage of β^+ (β^+ %) describes the portion of positron emission during the decaying process, the branching ratio. In [^{18}F] decay schema only 97 % is positron emission and 3 % is electron capture. The portion of electron capture is dependent on the decaying nucleus and it varies from 0% to 43% (in ^{64}Cu) for positron emitters used in PET. The electron capture means that the atomic nucleus captures an inner orbit electron and a proton converts to a neutron. Neutrino is emitted from the nucleus as a result. As an electron is captured from the inner K-shell, it leaves a hole in the orbit behind. The atom with a gap in its electron structure repairs itself by emitting x-rays or Auger's electrons. The nucleus may also stay in an excited state after the electron capture causing it to release desexcitation gamma rays. All these radiation processes cause extra absorbed dose in tissue without increasing the signal to PET imaging.

The maximum positron energy of [^{11}C] decay (0.96 MeV) is higher than the maximum energy of [^{18}F] decay (0.64 MeV). The positron undergoes multiple direction-changing interactions with electrons prior to annihilation and the total path length the positron travels is considerably longer than the positron range. The positron that is ejected following β^+ decay has a very short lifetime in electron rich material such as tissue. It rapidly loses its kinetic energy in inelastic interactions with atomic electrons in the tissue, and once most of its energy is dissipated (typically within 10^{-1} to 10^{-2} cm, depending on its energy), it will combine with an electron and form a hydrogen-like state known as positronium. This state lasts only about 10^{-10} seconds before annihilation occurs (Cherry & Dahlbom, 2004). As the positrons are absorbed locally they form the primary source of the radiation absorbed dose to subjects in PET imaging.

The 511 keV photons emitted following annihilation interact with the tissue surrounding them. The dominant form of interaction in tissue is Compton scattering (Cherry & Dahlbom, 2004).

2.6 Radiopharmaceuticals

Radiopharmaceuticals are biologically active molecules labelled with radionuclides. The molecules' specific interaction on the cell level defines the biodistribution in the body. For example, uptake of a certain radiopharmaceutical can be higher in tumors and metastases because of their exceptional interaction as compared to normal tissue cells. Different types of compounds, namely pharmaceuticals, neurotransmitters, proteins and other biomolecules involved in organ physiology processes, can be labelled with radionuclide and they are called radiopharmaceuticals.

Radiopharmaceutical production for PET begins with the bombardment of an appropriate target with accelerated particles produced with a cyclotron.

Alternatively, radionuclides can be obtained from radionuclide generators. Cyclotron produced precursors are [^{11}C]-CO_2, [^{11}C]-CH_4, [^{18}F]-F_2, [^{18}F]-$F^-_{(aq)}$ or [^{15}O]-O_2. [^{68}Ga] is typically produced with the ^{68}Ge/^{68}Ga generator.

The [^{11}C] is available as [^{11}C]-CO_2 ([^{11}C]-carbondioxide) or [^{11}C]-CH_4 ([^{11}C]-methane) from a medical cyclotron by the ^{14}N(p,α)^{11}C nuclear reaction. The [^{11}C]-CO_2 gas is widely used to produce ^{11}C-labelled precursors (Tu & Mach, 2010). In order to label organic target molecules with carbon-11, the [^{11}C]-labelled precursor is first typically converted to either [^{11}C]-methyl iodide ([^{11}C]-CH_3I) or [^{11}C]-methyl triflate ([^{11}C]-CH_3OTf). The labelling precursors [^{11}C]-CH_3I and [^{11}C]-CH_3OTf are used in [^{11}C]-methylation reactions to produce radiopharmaceuticals (Tu & Mach, 2010).

[^{18}F] production with a medical cyclotron is, generally, done by the ^{18}O(p,n)^{18}F nuclear reaction. If the target is [^{18}O]-enriched water, an aqueous solution of [^{18}F]-fluoride, [^{18}F]-$F^-_{(aq)}$ is produced. If target is [^{18}O]-O_2 gas, [^{18}F]-F_2 is produced. [^{18}F]-fluoride is produced as a reagent for nucleophilic labelling, whereas [^{18}F]-fluorine is produced for electrophilic methods (Jacobson et al., 2015). Electrophilic [^{18}F]-F_2 has low molar activity because [^{19}F]-F_2 gas must be added as a carrier to extract the [^{18}F]-F_2 from the target. Most of the fluorination reactions in nuclear medicine use nucleophilic [^{18}F]-fluoride as a labelling reagent usually introduced by S_N2 mechanism into aliphatic positions or via nucleophilic aromatic substitution into aromatic molecules. For [^{18}F], the fluorination methods include nucleophilic substitutions, fluoroalkylations, electrophilic substitutions and electrophilic addition reactions. For [^{11}C] the methods are mostly S_N2 methylations on O and N atoms.

The desired radiopharmaceutical is purified from side-products and a radiopharmaceutical solution suitable for intravenous injection is prepared. The final product must be sterilized and its quality checked before injection to living objects.

The best known radiopharmaceutical in PET imaging is 2-deoxy-2-[^{18}F]-fluoro-D-glucose, [^{18}F]FDG. It depicts glucose metabolism in cells and can be used for tumor and metastasis diagnostics, cancer staging and monitoring cancer therapy response. However, [^{18}F]FDG is a non-specific radiopharmaceutical and its uptake is higher in normal tissues with increased glucose metabolism, like heart muscle and brain and in tissues, exposed to inflammation.

Special PET radiopharmaceuticals are developed for diagnostics and follow-ups of treatment effects in patients with oncological, neurological, cardiovascular and inflammatory diseases. For example [^{11}C]methionine for detection of brain tumor, [^{11}C]raclopride for neuro receptor, [^{11}C]acetate for myocardial metabolism and [^{18}F]-FDOPA for investigation of normal and pathological dopamine metabolism in the human brain and tumors. The radiation exposure for all these radiopharmaceuticals mentioned above are reported in ICRP-publications (ICRP, 2015).

For cancer research and diagnostics, our novel radiopharmaceuticals ([^{18}F]FETNIM, [^{11}C]MeAIB, [^{11}C]choline and [^{18}F]-rhPSMA-7.3) were synthesized and evaluated in this thesis. Background for their development is given below in brief.

[^{18}F]FETNIM

Varying amounts of hypoxic cells exist in almost all solid tumors. These cells are known to be resistant to various forms of cancer therapy (Hall et al 1994). The clinical challenge is to detect the proportion of hypoxia accurately and feasibly to administer treatment specifically targeting poorly oxygenated cells (Brown et al 2000, Chapman et al 1998). [^{18}F]Fluoroerythronitroimidazole ([^{18}F]FETNIM) is one of the promising radiopharmaceuticals for imaging hypoxia *in vivo* using PET. (Yang et al 1995). The reductive metabolism of a nitroimidazole compound such as [^{18}F]FETNIM is associated with the activation and subsequent formation of covalent bonds with cellular macromolecules under hypoxic conditions. Thus, this compound tends to accumulate in sites of hypoxia and is therefore a potential candidate for imaging (Grönroos et al 2001).

Other hypoxia radiopharmaceuticals that have been studied are [^{18}F]FMISO ([^{18}F]fluoromisonidazole) (Graham et al., 1997), [^{18}F]-FAZA ([^{18}F]fluoroazomycin-arabinofulanoside) (Savi et al., 2017), [^{18}F]FETA ([^{18}F]fluoro etanidazole, preclinical only) (Barthel et al., 2004), [^{18}F]EF5 (Lin et al., 2012), [^{18}F]EF3 (Mahy et al., 2008), [^{18}F]EF1 (preclinical only) (Evans et al., 2000), [^{124}I]IAZA ([^{124}I]iodoazomycin arabinoide) (preclinical only) (Reischl et al., 2007), [^{64}Cu]ATSM (Kim et al., 2009), [^{18}F]HX4 (Doss et al., 2010), [^{18}F]FBNA ([^{18}F]benznidazole) (Nario et al., 2022), [^{18}F]RP-170 and [$^{60\text{-}64}$Cu]ATSM (Huang et al., 2021) and [^{18}F]DiFA (Watanabe et al., 2019). ^{68}Ga-labelled PET/CT hypoxia markers are under development. Possible candidates are [^{68}Ga]nitroimidazoles (Bresser et al., 2021). The most commonly used and extensively studied radiopharmaceutical for hypoxia imaging is still [^{18}F]FMISO (Bresser et al., 2021).

A list of publications for hypoxia radiopharmaceuticals which radiation dosimetry have been studied in humans is given in Table 5.

Table 5. Dosimetry studies on PET hypoxia markers.

Radiopharmaceutical	Effective dose coefficient [μSv/MBq]	Reference
[^{18}F]FMISO	13	(Graham et al., 1997)
[^{18}F]EF5	18 ± 2	(Lin et al., 2012)
[^{18}F]FAZA	13 ± 4	(Savi et al., 2017)
[^{18}F]HX4	27 ± 2 *	(Doss et al., 2010)
[^{18}F]DiFA	14 ± 0.7	(Watanabe et al., 2019)
[^{60}Cu]ATSM	11	(Laforest et al., 2005)
[^{64}Cu]ATSM	36	(Laforest et al., 2005)
[^{18}F]FETNIM	19 **	(Tolvanen et al., 2002)

* The effective dose coefficient for [^{18}F]HX4 (27 μSv/MBq) is high because urine voiding interval of 4.8 hours was used. If patients void in 1-hour intervals the effective dose coefficient is 14 μSv/MBq.
** The effective dose coefficient for [^{18}F]FETNIM (19 μSv/MBq) was measured with 4-h voiding interval. If patients void in 1-hour intervals the effective dose coefficient is 15 μSv/MBq.

[^{11}C]MeAIB

[*N*-methyl-^{11}C]α-methylaminoisobutyric acid ([^{11}C]MeAIB) is a metabolically stable amino acid analogue, which is transported across the cell membrane by system A (Christensen, 1990). System A is a hormonally regulated ubiquitous transport mechanism for neutral amino acids. It is energy dependent and can actively pump substrates against a concentration gradient from plasma into cells. Malignant transformation is associated with enhanced system A activity (Weber et al., 1984), which makes [^{11}C]MeAIB a potential tumorseeking agent for PET imaging. This is a major difference compared to [^{11}C]methionine, which prefers system L as the predominant transport route. [^{11}C]MeAIB and [^{11}C]methionine may be applicable for tumor diagnosis, since system A and L are both involved in transport of amino acids in neoplastic tissues.

Radiation dosimetry for a [^{11}C]-labelled radiopharmaceutical for PET imaging of system A amino acid transport has not been published prior to our research (Tolvanen et al., 2006). For [^{11}C]methionine the effective dose is 5.2 ± 0.5 μSv/MBq (Deloar et al., 1998).

[^{11}C]Choline

Malignant transformation is associated with the induction of choline kinase activity, which results in increased levels of intracellular phosphorylcholine, a key

intermediate in the biosynthesis of phosphatidylcholine. Choline-based phospholipids are formed in the S phase of the cell cycle when DNA is synthesized. Tumor cells, due to being rapidly proliferating cells, contain large amounts of phospholipids, particularly phosphatidylcholine (Zeisel, 1996); (Ramírez de Molina et al., 2002). [^{11}C]Choline is phosphorylated to [^{11}C]phosphorylcholine by choline kinase and trapped inside cells (Katz-Brull & Degani, 1996). [^{11}C]Choline and its fluorinated alternative [^{18}F]choline have been mainly applied in imaging for prostate cancer (Wibmer et al., 2016) before PSMA targeted agents became available.

In addition to our [^{11}C]choline dosimetry publication, there is only one abstract in the Journal of Nuclear Medicine about [^{11}C]choline dosimetry by Nosske and Brix, 2009, (Nosske & Brix, 2009). They reported an effective dose of 3 mSv from a 740 MBq [^{11}C]choline injection. As choline can also be labelled with the [^{18}F]-isotope, the dosimetry for both [^{18}F]fluorocholine ([^{18}F]FCH) and [^{11}C]choline are tabulated in Table 6.

Table 6. Dosimetry studies on [^{11}C] and [^{18}F]choline.

Radiopharmaceutical	**Effective dose coefficient [µSv/MBq]**	**Reference**
[^{11}C]choline	4.1	(Nosske & Brix, 2009)
[^{11}C]choline	4.4	(Tolvanen et al., 2010)
[^{18}F]FCH	27.3 $\pm$ 7.3	(Degrado et al., 2002)
[^{18}F]FCH	18	(Giussani et al., 2012)
[^{18}F]FCH	14.2* or 12.7**	(Fabbri et al., 2014)
[^{18}F]choline	20	ICRP Publication***

*ICRP60 weighting factors, ** ICRP103 weighting factors, *** ICRP Publication in internet 2013, Forth addendum to ICRP Publication 53.

[^{18}F]-rhPSMA-7.3

Prostate-specific membrane antigen (PSMA) is a transmembrane enzyme that is overexpressed in prostate cancer cells compared to healthy tissue (Silver & Fair, 1997). Its intracellular catalytic site allows targeting with specific small-molecule inhibitors or antibodies that may subsequently become internalized (Ghosh & Heston, 2004). [^{18}F]-labelled radiohybrid PSMA, [^{18}F]-rhPSMA-7.3 is a promising radiopharmaceutical for the detection of primary prostate cancer and its metastases with PET. Since [^{18}F]FDG no other tracers have made such a rapid breakthrough in the clinics than [^{68}Ga]- or [^{18}F]-labelled PSMA-based compounds. These are

examples of specific tumor seeking radiopharmaceuticals with direct clinical application.

Previously published dosimetry studies in humans for PSMA-based compounds are given in Table 7.

Table 7. Dosimetry studies on PET PSMA radiopharmaceuticals.

Radiopharmaceutical	Effective dose coefficient [µSv/MBq]	Reference
[^{18}F]PSMA-11	12.8 ± 0.6	(Piron et al., 2019)
[^{18}F]JK-PSMA-7	10.9	(Hohberg et al., 2019)
[^{68}Ga]PSMA-11	16.6	(Demirci et al., 2018)
[^{68}Ga]HBED-CC	15.8	(Pfob et al., 2016)
[^{68}Ga]DOTA-DiPSMA	19.4 ± 1.7	(Zhang et al., 2022)
[^{64}Cu]PSMA	29.2	(Liu et al., 2021)
[^{68}Ga]PSMA-617	21	(Afshar-Oromieh et al., 2015)
[^{68}Ga]PSMA I&T	19.9 ± 0.9	(Herrmann et al., 2015)
[^{18}F]DCFBC	19.9 ± 1.3	(Cho et al., 2012)
[^{18}F]DCFPyL	17 ± 2	(Plyku et al., 2018)
[^{18}F]PSMA-1007	22	(Giesel et al., 2017)
[^{18}F]-rh-PSMA-7.3	14 ± 1	(Tolvanen et al., 2021)
[^{18}F]-rh-PSMA-7†	12.2* 26.6**	(Knorr et al., 2022)
[^{18}F]-rh-PSMA-7.3†	12.8* 21.7**	(Knorr et al., 2022)

† derived from preclinical data, * 1h bladder voiding interval, ** 3,5 bladder voiding interval

2.7 Ethical consideration, Declaration of Helsinki

All scientific medical research needs ethical approval from a local research ethical committee before commencing the study. Approval for research where the subjects are human participants is based on the Declaration of Helsinki, a formal statement of ethical principles published by the World Medical Association (WMA) to guide the protection of human participants in medical research (https://www.wma.net/policies-post/wma-declaration-of-helsinki-ethical-principles-for-medical-research-involving-human-subjects/). It was adopted in 1964 by the 18th WMA General Assembly in Helsinki. The fundamental principle is to respect the individual and their right to self-determination and to make informed decisions

regarding participation in the research, prior to and throughout the course of the research (Bruce-Chwatt, 1965).

Ethical approval for each animal study must be obtained from the Regional State Administrative Agencies in Finland. Animals are cared for following the Directives 2012/707/EU, 2014/11/EU by the European Parliament and the Council for the Care and Use on Laboratory Animals.

3 Aims

This thesis set out to investigate the radiation burden of four new radiopharmaceuticals in accordance with their further development as tumor seeking radiopharmaceuticals in oncologic patients. In addition, this thesis shows how the methodology and precision have changed over time with better scanners, imaging protocols and software algorithms.

The specific objectives of this thesis are:

I. To investigate the radiation exposure of [^{18}F] labelled radiopharmaceutical [^{18}F]FETNIM, which was synthetized for imaging hypoxic sub-volumes inside tumors with PET. MIRDOSE 3 software was used in dosimetry estimates.

II. To investigate the radiation exposure of [^{11}C] labelled radiopharmaceutical [^{11}C]MeAIB. Because this radiopharmaceutical shows high accumulation in the salivary glands, and salivary glands are not modelled in MIRDOSE 3 software, we specifically modelled these tissues with spheric phantoms in order to estimate absorbed dose coefficients for salivary glands.

III. To investigate the radiation exposure of [^{11}C] labelled choline. This study compared the absorbed and effective dose coefficients obtained from measurements in rodents and humans.

IV. To investigate the radiation exposure of [^{18}F] labelled [^{18}F]-rhPSMA-7.3. This radiopharmaceutical has been described as a game changer in prostate cancer imaging in PET. A modification from the original PSMA molecule was the focus of our dosimetry investigation. A new bioimaging technique with state-of-art PET/CT scanner was applied and dosimetry was calculated with OLINDA/EXM 1.0 software.

4 Materials and Methods

4.1 Radiopharmaceutical preparation

The radiopharmaceuticals, [^{18}F]FETNIM, [^{11}C]MeAIB, [^{11}C]choline and [^{18}F]-rhPSMA-7.3, were produced on site at Turku PET Centre as described in publications.

Table 8. Radiopharmaceuticals used in this study.

	Abbreviation	**Chemical name or description**	**Reference for radiopharmaceutical production**
Study I	[^{18}F]FETNIM	4-[^{18}F]fluoro-2,3-didihydroxy-1-(2'-nitro-1'-imidazolyl)butane	(Yang et al., 1995), (Grönroos et al., 2001)
Study II	[^{11}C]MeAIB	[*N*-methyl-^{11}C]α-methylaminoisobutyric acid	(Någren et al., 2000)
Study III	[^{11}C]choline	Methyl-[^{11}C]-choline	(Roivainen et al., 2000)
Study IV	[^{18}F]-rhPSMA-7.3	radiohybrid prostate-specific membrane antigen	(Wurzer et al., 2021)

[^{18}F]FETNIM was synthesized from 1-(2'-nitro-1'-imidazolyl)-2,3-*O*-isopropylidene-4-tosyloxybutane by nucleophilic displacement of the tosyloxy group with [^{18}F]fluoride ([^{18}F]$F^-_{(aq)}$) followed by acidic hydrolysis of the diol-protecting group. The precursor for [^{18}F]FETNIM was prepared and the original synthesis method was reported by Yang et al. (Yang et al., 1995). The modifications from the original labelling method, which were used in the Radiochemistry laboratory at Turku PET Centre are given in detail by Grönroos et al 2001(Grönroos et al., 2001).

[^{11}C]MeAIB was prepared from the reaction of [^{11}C]methyl triflate with α-amino-isobutyric acid AIB methyl ester, generated *in situ* from its corresponding hydrochloride, followed by hydrolysis of the ester function with aquenous NaOH. Details for the [^{11}C]MeAIB synthesis with the chemicals and reaction times and equipment used during the synthesis are given by Någren et al 2000 (Någren et al., 2000).

[^{11}C]Choline was prepared from *N,N*-dimethylethanolamine and [^{11}C]methyl triflate. The chemical processes for how the [^{11}C]CO_2 was converted to [^{11}C]methyl iodide and further to [^{11}C]methyl triflate, as well as all chemical compounds needed for labelling *N,N*-dimethylethanolamine are given in the publication by Roivainen et al. 2000 (Roivainen et al., 2000).

[^{18}F]-rhPSMA-7.3 was prepared with a single-use cassette-based proprietary automated synthesis platform. Casettes are a new technology to make the creation of routine and research radiopharmaceuticals easier as it does multiple chemical reactions, radiolabelling, purification and formulation in a standardized way. For [^{18}F]-rhPSMA-7.3 the [^{18}F]$F^-_{(aq)}$ was used with Ga-rhPSMA-7.3 precursor as starting materials (Wurzer et al., 2021).

4.2 Subjects

All studies were conducted according to the principles of the Declaration of Helsinki. The study protocols were approved by the joint Ethics Committee of the University of Turku and Turku University Hospital. Each human subject provided informed consent before entering the study.

The biodistribution on the radiopharmaceuticals in humans was measured with dynamic PET scanning. The study protocol in studies I-III included dynamic scans of the thorax or abdominal area. In addition biodistribution data from previous PET studies were utilised if available. In study IV the state-of-art PET/CT scanner was used with series of dynamic whole body imaging protocol. Urine samples were collected from all subjects to calculate excretion of the radiopharmaceutical into the urine. The amount of radioactivity in urine samples was measured with a well-counter and corrected for decay. Calibrated results were expressed as kBq/ml in urine.

In study III nine Sprague-Dawley rats (Harlan, Indianapolis, IN) were used *ex vivo* and four athymic Hsd:RH-rnu/rnu rats (Harlan, The Netherlands) were scanned *in vivo*.

Table 9. Demographics of the study subjects.

	Number of subjects	**Age of subjects, mean ± SD**	**Injected activity, [MBq]**	**Weight of subjects, mean ± SD**
Study I	6 + 14* + 3**+ 4***	NA	366 (range 288-385)	NA
Study II	14	58 ± 11 years	422 (range 295-493)	79 ± 13 kg
Study III	6, 4****	60 ± 10 years, 6 weeks****	423 (range 328-466), 33 (range 19-47)****	78 ± 19 kg 354 ± 50 g****
Study IV	6	54 ± 16 years	220 (range 210-228)	78 ± 8 kg

* Dynamic data from neck muscle. **Dynamic data from brain. ***Urine samples only. ****Animal data.

4.3 PET imaging

4.3.1 Study protocol in study I, [^{18}F]FETNIM dosimetry

Studies were performed with an GE Advance PET scanner (GE Medical Systems Milwaukee, WI) operated in 2-dimensional mode. Before the injection the attenuation was measured with two rotating [^{68}Ge] rod sources for 10 minutes in each subject. Dynamic scans started immediately after the injection. Three different study protocols were used. In protocol 1 (dynamic scans of thorax and abdominal region) the frame rates were as follows: 8 x 15 s, 28 x 60 s and 6 x 200 s, total duration 50 minutes.

For dynamic scans of the head and neck region two different protocols were used since data was originally measured for cancer study purposes. In protocol 2 two emission parts included the frame rates as follows: 4 x 30 s, 3 x 60 s, 5 x 180 s, 8 x 300 s and and 6 x 600 s, break for 40 minutes and continue with 3 x 400 s frames, total session duration 3 hours.

In protocol 3 three emission parts included frame rates and breaks as follows: 4 x 30 s, 3 x 60 s, 5 x 180 s, break 60 min, 4 x 600 s, break 90 min, 3 x 600 s, total session duration 4 hours.

Patients were allowed to stand up and relax between scanning sessions if there was a break between scans. The same attenuation correction was used after careful repositioning with skin marks and positioning laser lines.

Urine samples were taken at 27 – 270 minutes after injection. Subjects were asked to empty their bladder after each emission scan. The time table for samples deviates because of the different emission duration in scanning protocols.

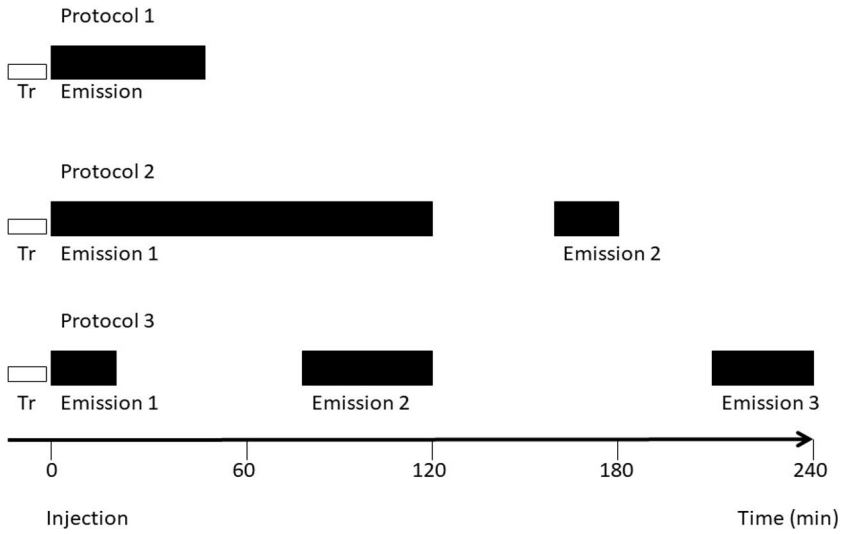

Figure 4. Three different scanning protocols were used in study I for [^{18}F]FETNIM biodistribution measurements. All imaging protocols started with a transmission scan, Tr. Protocol 1 was used to scan thorax and abdominal regions, protocol 2 and 3 were used in head and neck cancer patients. Frame rates varied in different protocols and are explained in the text above.

4.3.2 Study protocol in study II, [^{11}C]MeAIB dosimetry

Data from three different PET scanning protocols were used for [^{11}C]MeAIB dosimetry estimates. Studies of the abdominal or head and neck region were performed with the GE Advance PET-scanner operated in a 2-dimensional mode. The abdominal region was analysed in four subjects, including data from heart, lung, liver, kidneys, spleen, pancreas, stomach, red bone marrow and back muscles. Protocol 1 for imaging the abdominal region was designed as follows: 8 x 15 s, 6 x 30 s, 5 x 180 s and 4 x 300 s, total duration 40 minutes.

[^{11}C]MeAIB uptake in skeletal muscle was measured with a 2-dimensional ECAT 931/08 PET scanner (CTI Inc., Knoxville, TN) in 11 healthy volunteers. Originally the [^{11}C]MeAIB uptake into the anterolateral femoral muscle was studied in both the fasting state and during euglycaemic hyperinsulinaemia. Dosimetry estimations were made from both states per each participant, yielding 22 femoral muscle data sets. Protocol 2 for imaging femoral muscles included frames as follows: 8 x 30 s, 4 x 60 s, 1 x120 s and 4 x 300 s, total duration 30 minutes.

In protocol 3, imaging data from salivary glands of 14 cancer patient were used. Time frames of the scans were: 12 x 15 s, 4 x 30 s, 3 x 60 s, 1 x 120 s and 8 x 300 s, total duration 50 minutes.

Fifteen urine samples were collected in these [^{11}C]MeAIB studies between 29 - 79 minutes after injection.

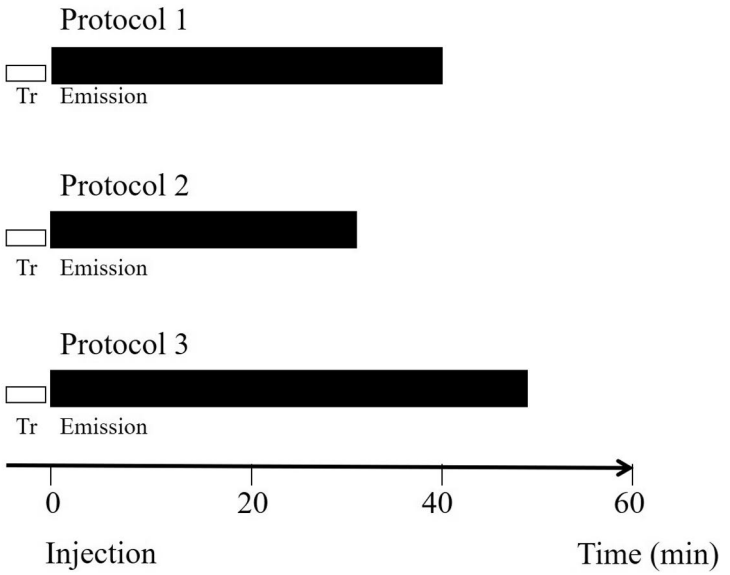

Figure 5. [^{11}C]MeAIB study protocols.

4.3.3 Study protocol in study III, [^{11}C]choline dosimetry

Human studies were performed with the GE Advance PET scanner operated in 2-dimensional mode. PET studies started with the attenuation measurement, followed by the [^{11}C]choline injection and the dynamic scanning. The time frames in thorax for 3 subjects or abdominal for 3 subjects were as follows: 8 x 15 s, 6 x 30 s, 5 x 180 s and 4 x 300 s, total duration 40 minutes. Data was derived from cortical bone, heart, kidneys, liver, lungs, muscle, pancreas, spleen, stomach and upper large intestine.

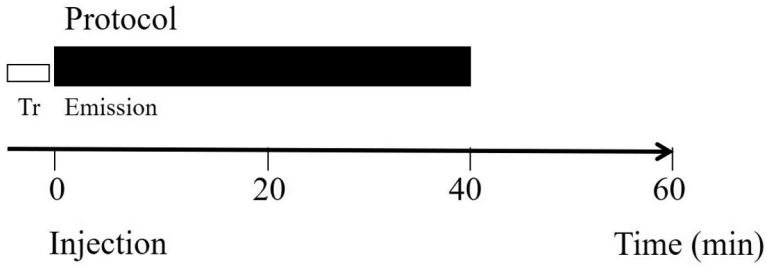

Figure 6. [^{11}C]Choline PET imaging protocol in human studies.

Preclinical *ex vivo* biodistribution data was measured at 5 min, 10 min or 15 min after injection in nine rats. Tissue samples were rapidly excised and blood collected.

The samples were weighed and measured for radioactivity in a well-type gamma counter (3¨ x 3¨ NaI(Tl) crystal).

Time frames of the *in vivo* dynamic scanning protocol in rat studies was 6 x 60 s and 10 x 300 s, total duration 60 minutes. PET studies were performed with an HRRT PET scanner (CPS Siemens, Knoxwille, TN), which had a 25.2 cm axial field of view. Transmission scan duration was 5 minutes and the whole animal was scanned with the same bed position. These dynamic scans produced data from rat heart, kidneys, liver, lungs, muscle, pancreas, spleen and upper large intestine.

4.3.4 Study protocol in study IV, [^{18}F]-rhPSMA-7.3 dosimetry

The whole body PET/CT, GE Discovery MI (GE Medical Systems, Milwaukee, WI) was used for human [^{18}F]-rhPSMA-7.3 biodistribution measurements. Since quick attenuation scan with the computed tomography (CT) was possible, a scan of the whole body was acquired. The PET scanning protocol included three sessions with breaks in between. The first session started with the whole body CT attenuation scan, followed by six PET scans with 7 bed positions (vertex to mid-thigh) or 13 bed positions (vertex to feet) and framed as follows: 30 s per position, break 150 s, 60 s per position, break 120 s, after that repeating 120 s per position scan and break 120 s twice. Scan number 5 in first session was from vertex to feet including 13 bed positions 120 s per bed position. Last 120 s per position scan in first session was from vertex to mid-thigh, seven bed positions.

The second session started after a 60-minute break. The subject was allowed to stand up, urine was collected and urine sample radioactivity was measured during this break. The subject was carefully repositioned at the same vacuum mattress as in the first imaging session. The second session included seven bed positions with 240 s scan per bed. After another 42-minute break, the subject was again repositioned to the vacuum mattress and the third scan session started, including 240 s scans in seven different bed positions. The total duration of the scanning session was 4 hours 8 minutes.

Session	Scan	Duration per Axial FOV (min)	Total duration (min)	Start time (min)	End time (min)
I	**1**	0.5	3.5	1	4.5
	Break			2.5 min	
	2	1.0	7	7	14
	Break			2 min	
	3	2.0	14	16	30
	Break			2 min	
	4	2.0	14	32	46
	Break			2 min	
	5	2.0	26	48	74
	Break			2 min	
	6	2.0	14	76	90
Break				60 min	
II	**7**	4.0	28	150	178
Break				42 min	
III	**8**	4.0	28	220	248

Figure 7. In PET scans 1-4 and 6 the axial extent was starting from vertex to mid-thigh (7 bed positions; variable time per bed position) and in PET scan 5, axial extent was from vertex to feet (13 bed positions; 2 minutes/bed). In PET scans 7 and 8 the axial extent was from vertex to mid-thigh (7 bed positions; 4 minutes/bed).

Biodistribution data was available from muscle, liver, lungs, heart wall, heart chamber content, kidneys, brain, breasts (women only), spleen, stomach, urinary bladder content, thymus, cortical bone, trabecular bone, salivary glands, lacrimal gland, upper and lower intestine content, small intestine content, adrenals and testes (men only).

4.4 Data processing

4.4.1 Image reconstruction

In this thesis human PET imaging data was collected with three different PET scanners. All PET scanners were cross-calibrated with a dosecalibrator (VDC 402 or VDC 405, Veenstra Instruments, the Netherlands) so that the measured true coincidence counts were converted into unit kBq/ml in images.

The oldest scanner, ECAT 931/08, which was used only for femoral muscle measurements in [^{11}C]MeAIB study, had a 10.8 cm axial field of view with 15 image slices. A transaxial field of view was 58 cm. An image matrix of 128 x 128 was used

with a filtered-back projection (FBP) reconstruction algorithm and a pixel size was 3.35 x 3.35 mm. This scanner was operating in 2-dimensional mode only.

Another scanner, GE Advance had a 15.2 cm axial field of view, 35 image slices spaced by 4.25 mm and a 55 cm transaxial field of view. The image matrix in abdominal region in [^{18}F]FETNIM, [^{11}C]MeAIB and [^{11}C]choline studies was 128 x 128, yielding to pixel size of 4.29 x 4.29 mm. The transaxial field of view in [^{18}F]FETNIM and [^{11}C]MeAIB head and neck cancer studies was 30 cm, yielding to pixel size of 2.34 x 2.34 mm. The FBP reconstruction algorithm was used in [^{18}F]FETNIM and [^{11}C]MeAIB studies, while an iterative ordered-subsets expectation maximization (OSEM) algorithm was used in [^{11}C]choline studies.

The third scanner was PET/CT Discovery MI, which was operating in 3-dimensional mode only. The axial field of view was 20.0 cm and simultaneous 71 image slices were reconstructed with an iterative 3D maximum likelihood ordered subset expectation maximization algorithm that uses time-of-flight information (VUE Point Fx). The image matrix of 192 x 192 was used in 70 cm transaxial field of view, yielding to 3.64 x 3.64 mm pixel size.

All PET images were corrected for the annihilation gamma photon's attenuation in the tissue. The scattered coincidences were not yet corrected in early PET scanners like in ECAT 931/08, which were used here in femoral muscle studies. For other PET images in this research the reconstruction algorithm corrects for scatter and random coincidences.

4.4.2 Region of interest

The time course of radioactivity concentration was measured from dynamic quantitative PET images. Region of interest (ROI) or volumes of interest (VOI) were manually defined on source organs in 3 or 4 contiguous image planes in each subject. The average pixel value in adjacent image planes was assumed to represent the radioactivity concentration in the whole organ.

For better visualization of the radiopharmaceutical biodistribution, the perfusion or the accumulation, dynamic PET images were summed. Early frames of dynamic image set were summed for organs of high perfusion and late frames summed images were used to visualize the source organs with clear accumulation compared to the background radioactivity. The outline of the source organs was readily visible on the summed PET images in most cases. Attenuation correction maps were used to position the ROI in vertebral regions. In study IV the CT images were used as an anatomical reference during the VOI definition. In studies I-III the GE analysis software was used and for study IV the Carimas software (Turku PET Centre, Finland) was used in defining the VOIs. After these operations the ROI or VOI was copied into the dynamic image set.

The main source organs for dosimetry calculation software were; brain, stomach, upper large intestine, heart chamber content, kidney, liver, lungs, muscle, pancreas, red marrow, spleen. Also ROI or VOI was drawn over gallbladder content, salivary glands, lacrimal glands, heart wall, breasts (women only), thymus, cortical bone, trabecular bone, lower large intestine content, small intestine content, uterus (women only), thyroid, adrenals and testes (men only) if those organs were visible in CT or PET images.

In PET the radioactivity accumulation is important, so the physical decay must be corrected into the time of injection. For dosimetry calculations only the real number of disintegrations is of interest. For that reason in MIRD schema non-decay corrected data is used.

4.4.3 Time activity curve

The time activity curve (TAC) was generated by copying the ROI or VOI drawn as described above to the dynamic PET image set. For analysis the time point in TAC was set in the middle of each scanning frame. The dynamic acquisition protocol must be designed so that physical half-life of the radionuclide and the biological half time of radiopharmaceutical are considered. For this purpose the effective half-time for the radiopharmaceutical (T_e) in a tissue is formulated as a function of physical half-life ($T_{½}$) and biological half-time (T_b):

$$T_e=(T_b x T_{½})/(T_b+T_{½}) \quad \text{(Eq 9)}$$

The overall acquisition time for reliable TAC should be five times the effective half-time of the radiopharmaceutical. If a mathematical fitting is used for TAC estimation, a general protocol could involve one or two data points taken at some fraction of effective half-time; one near effective half-time and one or two other data points taken at approximately 3 x effective half-time and 5 x effective half-time. (MIRD Pamphlet 16). On the other hand the data collection time should not exceed 5 x physical half-life, since the amount of true coincidence counts is not producing an accurate signal for image reconstruction anymore.

The number of datapoints in TAC is dependent on the framing and duration of the dynamic PET acquisition. In the beginning of the acquisition, short frames were optimal since there was a high concentration of the PET radiopharmaceutical in blood and rapid changes in accumulation took place immediately after administration of the radiopharmaceutical. Organs with effective blood flow are exposed to higher radiation burden during early frames. In later phases, longer frames are optimal to get better true coincidence counts statistics from low radioactivity concentration organs.

My experience in dosimetry measurements was that the effective half-time reduces the retention in source organs and shorter acquisition time was enough, for example, 40 minutes in a [^{11}C]MeAIB muscle scan. As the TAC was suspected to decay with the mono exponential function after the maximal peak value, two or three data points were needed to estimate the function parameters (Siegel et al., 1999).

4.4.4 Data normalization

The radioactivity concentration was defined in source organs from human dynamic PET images as a function of time. This provided time activity curves in each subject's source organs. For dosimetry calculation software the TACs were normalized to the reference adult weight and 1 MBq injection as follows:

$$C'(t) = C(t)\left(\frac{1}{A0}\right)\left(\frac{W}{W'}\right) \quad \text{(Eq 10)}$$

where C(t) is the measured radioactivity concentration from ROI or VOI analysis, A_0 is the injected activity (MBq), W is the subjects weight (kg) and W' is 70 kg.

The TACs from preclinical small animal ex vivo study were generated by normalizing data points with the following equation:

$$\left[\left(\frac{\%}{g organ}\right)_{animal} x(kgTBweight)animal\right] x\left(\frac{g organ}{kgTBweight}\right)_{human} = \left(\frac{\%}{organ}\right)_{human} \quad \text{(Eq 11)}$$

where $(g\ organ)_{animal}$ is the animal organ weight in grams, $(kgTBweight)_{animal}$ is the total body weight of the animal in kg, $(g\ organ)_{human}$ is the human organ weight in grams and $(kgTBweight)_{human}$ is the human total body weight, 70 kg (Kirschner et al., 1975). This equation converts rodents' data to human data assuming that the accumulation of the radiopharmaceutical at cellular level in both species is the same. The organ weight to total body weight ratio in humans was assumed to correlate to the organ weight to body weight ratio in rodents.

TAC's normalizations were done with the Microsoft Excel 2013 (Microsoft Office Professional 2013).

4.4.5 Excreta counting

Only the renal pathways were considered as an excretory route for the radiopharmaceuticals in these studies. Subjects were asked to empty their bladder before entering the PET scanning session. After the emission scanning the radioactivity in excreted urine was measured. The 2.5 ml sample of urine was measured in gamma well gamma counter (Bicron 3"x3" NaI(Tl) well counter, Bicron

Corp, updated by Hidex Oy, Turku, Finland) or in dosecalibrator (VDC-404; Veenstra Instruments, the Netherlands) and whole urinary bladder content was estimated by weighting the whole volume of voided urine. Percent of administrated radioactivity in voided urine was plotted as function of time after injection.

4.4.6 Fitting and extrapolation

Normalized TACs presented radioactivity per injected activity until the last measured time point. However, there was still radioactivity in the source organs after the last measured time point. TACs were fitted with the exponential function in Microsoft Excel 2013. Only the descending part of the TAC were used for fitting and the radioactivity after the last measured time point was assumed to continue in compliance with the fitted function until infinity.

4.4.7 Residence times

The residence time for the source organ was the ratio of the cumulated radioactivity (the total number of disintegrations) to the administered radioactivity. The unit for residence time was MBq-h/MBq. In this thesis residence times were calculated as area under the normalized and extrapolated TACs multiplied with the organ volumes derived from a 70 kg reference man. The direct integration with the trapezoidal method, which uses interpolation between the measured data points, approximates the area under the TAC as a series of trapezoids. Residence times for radiopharmaceuticals studied in this thesis are given in Table 10.

Table 10. Residence times for source organs in unit MBq-h/MBq.

Source organ	[^{18}F]FETNIM*	[^{18}F]-rhPSMA-7.3**	[^{11}C]MeAIB,	[^{11}C]choline,
Adrenals	-	0.0178	-	-
Brain	0.023	0.0051	-	-
Breasts	-	0.0051	-	-
Gallbladder content	-	0.0010	0.001	-
Lower large intestine	-	0.0064	-	-
Small intestine	-	0.0354	0.039	-
Stomach	0.009	0.0138	0.006	0.0067
Upper large intestine	0.012	0.0077	-	0.0074
Heart content	0.011	0.0342	0.006	0.0019
Heart wall	-	0.0123	-	-
Kidneys	0.033	0.2700	0.017	0.0210
Liver	0.152	0.4678	0.040	0.1140
Lungs	0.015	0.0268	0.006	0.0123
Muscle	1.060	0.4114	0.210	0.1510
Pancreas	0.006	0.0082	0.006	0.0099
Red marrow	0.053	0.0560	0.016	-
Cortical bone	-	0.0882	-	0.0405
Trabecular bone	-	0.0194	-	-
Spleen	0.013	0.0734	0.002	0.0049
Testes	-	0.0014	-	-
Thymus	-	0.0008	-	-
Thyroid	-	0.0010	-	-
Urinary bladder content	0.244	0.0089	0.001	0.0027
Uterus	-	0.0056	-	-
Lacrimal glands	-	0.0022	-	-
Salivary glands	-	0.0094, Submandibular 0.0142, Parotid 0.0041, Sublingual	0.001	-
Remainder of the body	0.760	-	0.150	0.1310

*4-hour voiding interval
** 3,5-hour voiding interval

4.5 Radiation dose calculations

Absorbed doses were calculated with the MIRD schema, which was developed for radiation dose calculations in internal exposure. The equation to the mean absorbed dose, D in a target organ r_k, from injected radioactivity A_0 is:

$$\frac{\overline{D}(r_k)}{A_0} = \sum_h \tau_h S(r_k \leftarrow r_h) \qquad \text{(Eq 12)}$$

where S value contains physical characteristics of selected radionuclide (half-life, emission types and energies, decay products and penetration ability of the radiation) and the specific fraction of absorbed energy from source organ r_h to target organ r_k. Residence time, τ_h includes the kinetics of the radionuclide in the source organ r_h. Mean absorbed dose is sum of absorbed doses from those source organs that contribute to the target organ.

Radiation doses in study I were calculated with the MIRDOSE 3 software (Oak Ridge Associated Universities, Oak Ridge, TN, US). The software converted absorbed doses to target organ equivalent doses and calculated the total body effective doses using w_T from the ICRP Publication 60 (Stabin, 1996). The second software version MIRDOSE 3.1 (Oak Ridge Associated Universities, Oak Ridge, TN, US) was used in study II. The same tissue weighting factors were included in the calculations.

The MIRDOSE software was completely rewritten by the same producer and the new software OLINDA/EXM 1.0 (Vanderbilt University, Nasville, TN, US) was published in 2004 (Stabin et al., 2005). OLINDA/EXM 1.0 software uses the same factors and human models as MIRDOSE 3.1, but it was written with Java (Sun Microsystems) programming language. This software was used in studies III and IV.

5 Results

All four studies produced absorbed dose coefficients and effective dose coefficients of novel radiopharmaceuticals. The critical organ for each radiopharmaceutical was also determined. Organ absorbed dose coefficients and effective dose coefficients for [^{18}F]FETNIM, [^{18}F]-rhPSMA-7.3, [^{11}C]MeAIB and [^{11}C]choline are compared in Table 11. In this comparison values from the 4-hour and the 3.5-hour voiding interval results were reported for [^{18}F]FETNIM and [^{18}F]-rhPSMA-7.3, respectively. Voiding interval was not considered in [^{11}C]MeAIB and [^{11}C]choline dosimetry calculations.

5.1 Studies I – IV

Table 11. Absorbed dose coefficients in mGy/MBq and effective dose coefficients in mSv/MBq for four different radiopharmaceuticals.

Target organ	[^{18}F]FETNIM *	[^{18}F]-rhPSMA-7.3 **	[^{11}C]MeAIB	[^{11}C]choline
Adrenals	0.012	0.184	0.0032	0.0036
Brain	0.006	0.002	0.0016	0.0011
Breasts	0.007	0.004	0.0017	0.0014
Gallbladder wall	0.014	0.017	0.0047	0.0045
Lower large intestine wall	0.014	0.007	0.0029	0.0018
Small intestine	0.012	0.012	0.0135	0.0023
Stomach	0.012	0.012	0.0053	0.0060
Upper large intestine wall	0.015	0.010	0.0038	0.0063
Heart wall	0.011	0.020	0.0038	0.0034
Kidneys	0.027	0.172	0.0167	0.0206
Liver	0.024	0.062	0.0078	0.0201
Lungs	0.008	0.010	0.0027	0.0046
Muscle	0.012	0.006	0.0030	0.0025
Ovaries	0.014	0.005	0.0033	0.0020
Pancreas	0.019	0.028	0.0184	0.0292
Red marrow	0.012	0.010	0.0036	0.0019
Bone surfaces	0.011	-	0.0030	-

Skin	0.007	0.002	0.0017	0.0012
Spleen	0.020	0.083	0.0045	0.0091
Testes	0.011	0.005	0.0019	0.0013
Thymus	0.009	0.010	0.0022	0.0017
Thyroid	0.009	0.010	0.0020	0.0015
Urinary bladder wall	0.127	0.012	0.0022	0.0034
Uterus	0.018	0.011	0.0032	0.0019
Lacrimal glands		0.08	-	-
Salivary glands	-	0.148, Submandibular 0.114, Parotid 0.065, Sublingual	0.0063	-
Total body	0.011	-	0.0029	0.0030
Effective dose coefficient	0.019	0.014	0.0040	0.0044

* voiding interval 4 hours
** voiding interval 3.5 hours

5.2 Study I

The excretion of [^{18}F]FETNIM into the urine was measured from 28 voided urinary samples from 27 different subjects. Excretion through the renal pathway ranged from 6% to 50% of injected activity during 250 minutes after injection. Considerable excretion into urine makes the urinary bladder wall a critical organ in [^{18}F]FETNIM PET studies. For the radiation dose estimation two voiding schedules, 2- and 4-hours, were used in MIRDOSE 3.0 software.

Other main sources regions were the kidneys, liver, spleen and blood. On PET images, these regions were visually found to contain more radioactivity than the rest of the body. Also, the stomach, pancreas and upper large intestine were detectable in some subject's PET images and these organs were included in dosimetric calculations. Lungs being large organs are easy to define in thorax PET images. Although the [^{18}F]FETNIM uptake in muslces was low, showing a maximal mean value of 0.015 kBq/ml, the muscle is an important source organ because of its large volume in the body. Special attention was given to the absorbed dose of red marrow, because it is sensitive to radiation. Bony structures were not directly visualized in [^{18}F]FETNIM PET images and the ROI was drawn on transmission images.

The time-activity curves are shown in study I Figures 2 and 3. Subject–to-subject variation in time-activity curves for the kidneys can be seen because of differences in normal renal function. This also explains the large variation in radioactivity excreted into urine. The organ absorbed dose coefficients for a 70 kg adult male are given in Table 11.

The highest absorbed dose coefficients were found for the urinary bladder wall, with 0.062 mGy/MBq or 0.127 mGy/MBq corresponding to the 2- or 4-h voiding

schedule, respectively. The effective dose coefficient was estimated to be 0.015 mSv/MBq or 0.019 mSv/MBq depending on the voiding schedule.

5.3 Study II

The [^{11}C]MeAIB excretion into urine was below 1.4% of the injected activity within 79 minutes post-injection for all subjects. The maximal mean uptake in kidneys, 0.12 kBq/ml, was based on the uptake of the [^{11}C]MeAIB into the renal cortex. Despite the heterogenous distribution in kidneys, the whole organ was considered as the source organ in dose calculations.

In addition to the renal cortex, the uptake in the pancreas, stomach and intestines was observed in abdominal PET scans. Liver uptake was mild, 0.06 kBq/ml, but it is a standard source organ in dosimetry calculations. The residence time in the liver was higher compared to the kidneys' residence time because of the heavier organ mass of the liver.

For dosimetric analysis of skeletal muscle, a previous data set from a study on system A amino acid transport was re-analysed. The [^{11}C]MeAIB concentration in anterolateral femoral muscle in 11 subjects during insulin stimulation and in the fasting state was included. The red marrow was also measured, even though bone structures were not visualized in PET images.

The highest absorbed dose coefficients were found in the pancreas 0.018 mGy/MBq, the kidneys 0.017 mGy/MBq and the small intestine 0.014 mGy/MBq. The dose coefficient to kidneys was overestimated because the radioactivity was accumulated mainly in the renal cortex and the ROIs were drawn on those areas. Despite this, the whole kidney was considered as a source organ and the mass of the reference man kidneys was used. The critical organ in [^{11}C]MeAIB PET studies was the pancreas.

Because the salivary glands are visible in [^{11}C]MeAIB PET images and they are not considered as source nor target organs in MIRDOSE 3.1 software, the absorbed dose coefficients to parotid glands and submandibular glands were estimated with spherical phantoms of the size of 20 g and 10 g, respectively. The average absorbed dose coefficient in parotid and submandibular glands (0.0063 mGy/MBq) was named as salivary glands in Table 11.

The effective dose coefficient of [^{11}C]MeAIB was 0.0040 mSv/MBq in 70 kg adult male.

5.4 Study III

The excretion of [^{11}C]choline into urine was below 2% of the injected activity up to 1.5 hours after injection in humans. *Ex vivo* biodistribution data from rats showed

that [^{11}C]choline distributed particularly into the kidneys, lungs, adrenal glands and liver. In human PET studies the main uptake was seen in the renal cortex, salivary glands, liver, spleen, pancreas, blood and muscles. Being aware of the sensitivity of the red marrow to radiation, we paid specific attention to the estimation of absorbed dose into red marrow.

The critical organ in the [^{11}C]choline PET study was the pancreas with an absorbed dose coefficient of 0.0292 mGy/MBq. The effective dose coefficient was estimated to be 0.0044 mSv/MBq in a 70 kg adult male derived from human measurements and 0.0028 mGy/MBq derived from preclinical studies. A remarkable discrepancy between rat- and human-derived absorbed doses was seen in the pancreas, stomach wall, kidneys, osteogenic cells, spleen, liver and urinary bladder wall. Rat-derived values were 60 % - 35 % lower compared to human-derived values. However, 70 kg adult person absorbed dose coefficients based on rat *ex vivo* measurement were higher in testes, brain, thyroid, uterus, skin and lower large intestine wall compared to absorbed dose coefficients based on human subject measurements.

5.5 Study IV

At the mean time of 111 minutes after injection, the mean results from the 6 subjects indicated that 7.2 % of the injected [^{18}F]-rhPSMA-7.3 was excreted into urine. Later timepoints reveal that 11.4 % and 14.8 % of injected activity was excreted into urine at 194 min and 263 min, respectively.

The organs with the highest mean absorbed doses per unit of administered radioactivity were the adrenals (0.184 mGy/MBq), the kidneys (0.172 mGy/MBq) and the submandibular glands (0.148 mGy/MBq). For dose calculations the dynamic voiding model was used with two voiding intervals, 1 hour and 3.5 hours. All organs were found to have the same absorbed dose coefficients despite the different voiding intervals, with the exception of the urinary bladder wall absorbed dose coefficient. It was 0.006 mGy/MBq with a 1-hour interval and 0.012 mGy/MBq with a 3.5-hour interval.

The salivary glands were not available as source or target organs in OLINDA/EXM 1.0 software. The absorbed doses to these organs and the lacrimal glands were estimated with spheric phantoms because the uptake of [^{18}F]-rhPSMA-7.3 was significant in dynamic PET images. The sphere sizes were 25 g for parotid glands, 12.5 g for sublingual salivary glands and submandibular salivary glands and 5 g for lacrimal glands. The effect of these small organs was not noticed in the whole body effective dose coefficient in OLINDA/EXM 1.0 software. The effective dose coefficient from [^{18}F]-rhPSMA-7.3 injection was 0.0138 mSv/MBq when 1 hour voiding interval was used and 0.0141 mSv/MBq with a 3.5 hours voiding interval.

5.5.1 Study IV re-calculation

During writing this thesis I found that in original calculation for [^{18}F]-rhPSMA-7.3 the residence time for remainder of the body (one source organ) was not included as input data in OLINDA/EXM 1.0 calculations. There was an error in published results. To compare the incorrect values with corrected values, doses are given in Table 12 below.

Table 12. Previous and re-calculated absorbed dose coefficients in mGy/MBq and effective dose coefficients in mSv/MBq for [^{18}F]-rhPSMA-7.3 in male phantom with 3.5 h voiding period.

	D WITHOUT REMAINDER OF THE BODY	D WHEN REMAINDER OF THE BODY INCLUDED
ADRENALS	0.184	0.175
BRAIN	0.002	0.003
SUBMANDIBULAR GLANDS	0.148	0.148
PAROTID GLANDS	0.114	0.114
SUBLINGUAL GLANDS	0.065	0.065
LACRIMAL GLANDS	0.080	0.080
BREASTS	0.004	0.007
GALLBLADDER WALL	0.017	0.023
LLI WALL	0.007	0.012
SMALL INTESTINE	0.012	0.023
STOMACH WALL	0.012	0.020
ULI WALL	0.010	0.017
HEART WALL	0.020	0.021
KIDNEYS	0.172	0.193
LIVER	0.062	0.065
LUNGS	0.010	0.012
MUSCLE	0.006	0.009
OVARIES	0.005	0.011
PANCREAS	0.028	0.032
RED MARROW	0.010	0.015
OSTEOGENIC CELLS	0.012	0.019
SKIN	0.002	0.006
SPLEEN	0.083	0.088
TESTES	0.005	0.011
THYMUS	0.010	0.012
THYROID	0.010	0.012
URINARY BLADDER WALL	0.012	0.016
UTERUS	0.011	0.011
TOTAL BODY	-	0.013
EFFECTIVE DOSE COEFFICIENT	0.014 mSv/MBq	0.018 mSv/MBq

6 Discussion

6.1 Dosimetry nomenclature

The two most used dosimetry methods in nuclear medicine are the MIRD schema and the ICRP method. The MIRD schema is focused on internal dose assessment of radiopharmaceuticals and the ICRP method was originally focused on radiation protection guidance. The dosimetry quantities used in these two methods are compatible and only the terminology differs. The dosimetry terms used in this thesis and in the original publications follow the MIRD schema.

The terms are exactly defined in the table in the publication MIRD Pamphlet 21 (Bolch et al., 2009). However, when reviewing nuclear medicine dosimetry publications there seems to be imprecision in using these terms. For example, the absorbed dose coefficient $d(r_T,T_D)$, where the absorbed dose is expressed per unit activity administered (Gy/Bq) is often written as absorbed dose in the literature. To be precise the absorbed dose in the target organ from a radiopharmaceutical $D_R(r_T,T_D)$ is the total dose from radiation exposure, which is the product of the absorbed dose coefficient and the injected activity A_0. The same imprecision appears within the use of the radiation protection terms equivalent dose coefficient $h(r_T,T_D)$ and equivalent dose to target $H(r_T,T_D)$. The effective dose coefficient is not mentioned as a MIRD term in the MIRD Pamphlet 21, wherein the effective dose coefficient is the effective dose per administered activity and the effective dose, E, total body dose is the product of effective dose coefficient and the administered activity.

The term residence time τ was used throughout in our original publications. The same quantity is currently expressed as the time-integrated activity coefficient $\tilde{a}(r_S,T_D)$.

6.2 Dose estimation accuracy

Radiation doses from internal exposure can not be measured directly with dosimeters. The complexity in estimating absorbed dose in organs comes from the variation in the amount of radioactivity and its spatial distribution. The estimation of internal exposure dose, i.e. absorbed dose, requires knowledge of the physical

properties of the radionuclide as well as knowledge of circumstances and biokinetics of the radiopharmaceutical inside the body. Physical properties for selected radionuclides are known constants. Circumstances inside the body, meaning volume and distance of the source and target organs, is modelled with reference human phantoms. Biokinetics can be measured for example with PET imaging technique. Variation in these quantities have an influence on dose estimation accuracy.

The accuracy of the absorbed dose calculation can be estimated by evaluating factors in the equation (Eq.2). The k, proportionality constant (Gy-kg/MBq-sec-MeV) is a constant value. The uncertainty in physical properties like in number of radiation, n_i, with energy, E_i, emitted per nuclear transition and uncertainty in the energy, E_i, per radiation is low and mostly negligible. The fraction of energy absorbed in the target, the mass of target region (kg) and cumulated activity in source organ (MBq-sec) contribute most of the uncertainty in an internal dose calculation (Stabin, 2008).

The S term in MIRD schema (Eq. 4) includes the proportionality constant k, characteristics of radionuclide ($T_{½}$, emission type and energies, decay products and penatration ability of the radiation) and the specific fraction of absorbed energy to each source- target organ pair, ϕ, and the target organ mass. The fraction of energy absorbed in the target from each source organ that contributes to absorbed dose is tabulated for different radionuclides. Monte Carlo software code is used in calculation of these fractions and the absolute uncertainty can be improved up to ~ 5% by repeating the iterations during ϕ calculation with modern computers (Stabin, 2008). However, variation in the mass of the target organ and variations in the distance between source and target organs are the major contributors to the uncertainty in S values (ICRP 128, 2015). Mattsson et al published in ICRP Publication 128 that experimental validation of calculated absorbed doses have indicated agreement within 20-60 % because of the S value uncertainty.

Masses of target and source organs are expressed for standardized individuals like reference man, reference woman or reference pediatric individuals. Subjects participating in PET studies vary essentially in body size and shape from these references. Human participants in our study design were planned to be as close to 70 kg as possible so that their body size and shape would fit the reference model. More realistic models of the body will replace present models in the future, but also these are designed to represent the median individual in a population.

The influence of the reference phantom size on the absorbed dose coefficient and effective dose coefficient for [^{18}F]FDG was studied by Carter et al (Carter et al., 2021). They used as biokinetic data the standard time-integrated activity coefficients for the brain, heart wall, lungs, liver, urinary bladder content and the remainder of the body from the ICRP 128 radiopharmaceutical data compendium in each phantom. Different fantom formats (stylized reference phantoms, voxel reference

phantoms, hybrid reference phantoms and current-generation mesh patient-dependent phantoms) were used to mimic different anatomy. The impact of height, weight and body contour variation in phantoms was assessed on [^{18}F]FDG dosimetry. As a result they found that detriment-weighted dose coefficients for the patient-size dependent phantoms varied by up to $\pm$ 40% relative to the corresponding reference phantom effective dose coefficients.

In general the uncertainty of dose estimation in internal dose calculation for radiopharmaceuticals is at least a factor of 2 when combining all uncertainties. The largest contributions to uncertainty are the phantom related parameters, ϕ, and target mass, the biokinetic parameters namely fractional uptake and effective half time in organs variation across individuals and variation in the w_T over time (Stabin, 2008).

In our studies the radiation dose calculations are based on measured biodistribution in living subjects. For the dose estimation calculations the primary data, the quantitative PET image, is generally thought to be accurate in measuring biokinetics. Some inaccuracy in biokinetics and time-activity curves is generated during the extrapolation of source organ uptake curves into infinity. The length of the dynamic PET acquisition should be long enough to detect the descendent phase of the source organ time-activity curve. If the curve is not turning down during the dynamic PET acquisition, the physical decay and radionuclide half-life is used as an approximation for TAC until infinity in the source organ. This yields an overestimation of the area under the curve and to the absorbed dose calculation because the biological washout is not considered.

6.2.1 Organ dimensions

During acquisition, PET measures radioactivity concentration Bq/ml. The tissue density of 1 g/ml is used to convert organ volumes to masses, because the organ quantities in the reference man, woman and child are given in grams. The density of lungs differs the most from that assumption, but the impact of density difference is negligible.

6.2.2 Number of source organs

The accuracy of radiation dose estimates for a new radiopharmaceutical increases as more uptake sites are defined in a subject. The first impression of the dose estimation can be based on the uniform distribution of the radionuclide in the selected reference phantom with the dose estimation software. Then, by adding biokinetic data from large organs like the liver, lungs, heart and kidneys will increase the precision of the estimation, while less amount of uniformly distributed radioactivity is in the remainder of the body. In studies I-III limited amount of TACs were available for

dosimetry calculations, since only images of the thorax or abdominal area was acquired per subject. However, the most interesting organs such as kidneys, liver, lungs, heart, stomach, pancreas and spleen were measured. The rest of the radioactivity was considered as remainder of the body radioactivity. In study IV dynamic whole body scanning became available with PET/CT, which increased the number of source organs since the range of the scanned body was larger. Also the statistics of TACs were improved while many different source regions could be measured in each subject. This provides a more accurate effective dose coefficient estimation.

Josefsson et al. (Josefsson et al., 2020) have concluded that there is a trade-off between the number of source organs considered, and the effort required to process the time activity curve for each organ needed for the calculations. They found that the number of organs required to reach the stability of effective dose coefficience is dependent on which order the source organs are included into the calculation. Also the importance of large organs, such as muscles or the remainder of the body, as a source term in calculations was mentioned.

As our results demonstrate the remainder of the body or the rest of the body is essential to include in the dose assessment calculations. The difference in effective dose coefficient was 23 % if the remainder of the body residence time was not given as input data into the internal dose calculation software.

6.3 Excretion of radioactivity into the urine

When the use of a new radiopharmaceutical is under consideration, one important detail is the excretion of radioactivity into urine. Variation may be from a few percent up to 70 % of the injected activity. It indicates immediately whether the radiopharmaceutical is excreted via the renal pathway and whether the urinary bladder wall is a candidate for being the critical organ. In our studies, the radiopharmaceutical excretion into the urine was 1.4 % and 50 % with [^{11}C]MeAIB and [^{18}F]FETNIM, respectively.

Patients or study subjects are adviced to drink more than usual and to void often after the PET study in order to minimize the radiation burden to the urinary bladder wall especially if the radiopharmaceutical is excreted into urine.

6.4 Realistic maximum doses

There is a realistic maximum model for the [^{11}C] radionuclide in ICRP Publication 106. With this model the effective dose coefficient in an adult for [^{11}C] is 0.011 mSv/MBq. The model assumes that 50 % of the decay occurs while the substance passes the urinary bladder, and the remaining 50 % of the disintegrations occur when

it is distributed homogenously within the whole body (ICRP, 2008). In our studies with [^{11}C]MeAIB and [^{11}C]choline the exeretion into urine was considerably lower. The effective dose coefficients were also lower compared to the realistic maximum for [^{11}C] radiopharmaceuticals. This is consistent with the safe application of [^{11}C]MeAIB and [^{11}C]choline in human subjects when using the injected activities applied in the current thesis.

ICRP Publication 106 announced that the realistic maximum model for [^{18}F] has been determined and is available, but it is not given in that document. For [^{18}F]-labelled brain receptor substances the ICRP 106 publication displays the effective dose coefficient for adult as 0.028 mSv/MBq. A total of 60 % of the administered activity is assumed to be excreted into urine and 40 % via the gastrointestinal tract. (ICRP 106, 2008). The absorbed doses and the effective dose coefficient of [^{18}F]FDG, the most used radiopharmaceutical in diagnostic PET studies, are often used as reference for [^{18}F] labelled radiopharmaceuticals. The effective dose coefficient for [^{18}F]FDG is 0.019 mSv/MBq (ICRP, 2015) which equals to that of [^{18}F]FETNIM if a 4-hour voiding schedule is used for the later. For [^{18}F]-rhPSMA-7.3 the effective dose coefficient is lower at 0.018 mSv/MBq. Again, the findings in the current thesis indicate that both [^{18}F]-labelled radiopharmaceuticals are safely administered in humans if administered activities are kept at the studied level.

6.5 Methodological considerations

6.5.1 PET scanning

In this thesis three different PET scanners were applied in human studies: Siemens ECAT 931-08 installed in 1988 (femoral muscle measurements only), GE Advance installed in 1996 and PET/CT GE Discovery MI installed in 2017 in Turku PET Centre. In dedicated whole body PET scanners, without the CT, the dosimetry studies were acquired in the thorax or abdominal area separately instead of whole body scanning. This was because of the slow-speed transmission measurement when the whole body was the target range. The transmission scans were done with the external radionuclide source and it took over 30 minutes to run the transmission scan for the whole body. Also, the whole-body emission scanning protocol, which has very short frames, was too demanding for the PET scanners in late the 1990's. The axial field of view was 15.2 cm for GE Advance. Hence it would have taken many bed positions to cover the whole body range from vertex to mid thighs with the scanner.

In state-of-art PET/CT GE Discovery MI the transmission was scanned in a few seconds with the CT scanner. This method was quick but had the disadvantage of an extra radiation dose from x-rays. The PET part has 20.0 cm axial field of view and

for the whole body scan from vertex to mid thighs, it took 6-7 bed positions. Nowadays data acquisition and reconstruction computers are powerful enough to deal with such an amount of data.

Two-dimensional (2D) mode, meaning lead intersepta between adjacent detector planes, was used in thorax and abdominal scans in PET Advance scanner. This scanner has bismuth germinate (BGO) scintillation crystals with the limited energy resolution and scattered photons cannot be completely rejected by energy discrimination. Intersepta reduces the rate of scattered counts but also reduces the sensitivity for true coincidence counts in 2D. If the Advance was used in 3D mode, the count rate would have been higher. However, the detector dead time would have been higher and the count rate for random coincidence countrate would have increased. These would have influenced image quality.

In Discovery MI this phenomen is resolved with software corrections such as randoms and fully 3D scatter corrections. The scanner is working only on three-dimensional mode and there is no intersepta needed between the adjacent detector rings. The Discovery MI has lutetium based scintillation (LBS) crystals and digital photomultipliers.This new detector design provides reduced randoms and shorter dead time and improved scatter rejection. The sensitivity for coincidence countrates is around four times higher and the noise to signal ratio in images is improved.

Even though PET scanning protocol design developed during our dosimetry project the gathered data from first studies is as reliable as data from the last study. The acquisition for each radiopharmaceutical has started immediately after injection and duration has been long enough to detect the descending part of the TAC. The quality of TAC has been good for fitting the data with exponential function.

6.5.2 Software based variation in calculations

The accuracy of dosimetric estimations is not restricted to the precision of PET methodology. The models of humans in calculation software code are not equal to subjects whose biodistribution is measured. For an adult male the body weight is 70 kg or 73 kg, for adult female 58 kg or 60 kg, depending on the calculation software in use. For children at different ages (15, 10, 5 and 1 year old) the body weight deviates. The models have developed over the decades and the new version of the software applies new reference person models. Previously dose factors have been based on anthropomorphic phantoms for adults, children and pregnant women, but phantoms are now replaced with realistic, image based voxelized models.

Monte Carlo studies establish absorbed fractions for electrons and photons for defined organ pairs. These provide more precise S values in the MIRD schema.

Salivary glands had high uptake of both [^{11}C]MeAIB and [^{18}F]-rhPSMA-7.3. The absorbed doses for these organs plus lacrimal glands for [^{18}F]-rhPSMA-7.3 were

calculated by modelling source and target organs with the spheric phantoms in OLINDA/EXM 1.0. Those absorbed doses were not included in the effective dose coefficient calculation since they are not included in the software versions before OLINDA/EXM 2.2. This was a major setback owing to the increased use of imaging tracers as a prelude to the theranostic approach, where the salivary gland absorbed dose may be critical. The sensitivity to radiation detriment should be studied and the w_T defined for salivary and lacrimal glands. Also the absorption fraction for the glands itself as well as the absorption fraction to adjacent organs is needed. The lack of this data underestimates the effective dose with radiopharmaceuticals having uptake in salivary or lacrimal glands.

6.5.3 Development in calculation factors

The calculation of effective doses has become more precise over 30 years, since the tissue-weighting factors w_T have been updated. The recommended numeric values for w_T have become more precise over this period as new information about cancer induction in various populations, like Japanese atom bomb survivors, has been reported.

The development of radiation weighting factor w_R has no influence on positron emitting radionuclides since the factor for gamma radiation and positrons has not changed.

6.5.4 Participants

Each person provided informed consent before entering the human study. Subjects were selected to be approximately 70 kg in order to reduce modification of TACs during the normalization process and because of the 70 kg reference model was used in calculations. There still was variation in weights of participants. It has low influence on calculated effective dose coefficients since participants both over and under 70 kg were recruited.

Study I includes 27 participants because previous PET scans with the [^{18}F]FETNIM were also included. All participants had a histologically verified cancer, but the normal tissues used for dosimetry were distant from the site of the tumor. The biodistribution of the [^{18}F]FETNIM in the whole body was assumed to be undisturbed by the hypoxi-spesific uptake.

Fourteen cancer patients in remission were included in study II. Normal tissues used for dosimetry were distant from the site of the tumor and biodistribution on [^{11}C]MeAIB in the whole body was assumed to be unaffected by the uptake of the previous tumor.

Study III includes six patients with rheumatoid arthritis. As dosimetric measurements were over thorax or abdominal region, organs were distant from the site of the inflammation. The [^{11}C]choline biodistribution was assumed to be undisturbed by the uptake in the inflamed joints.

Study IV was performed with six healthy volunteers. The biodistribution was assumed to correspond with the biodistribution of this radiopharmaceutical in a standard subject with normal physiology.

Finally, in each study only subjects with normal renal and liver function were recruited.

6.6 New radiopharmaceuticals

The safety of the administering a new radiopharmaceutical must be guaranteed during the development of said radiopharmaceutical. All radiopharmaceuticals in this thesis were studied for non-toxicity and the chemical and radiochemical purity was controlled before injecting into humans.

New radiopharmaceutical radiation safety can be determined by comparing the absorbed dose coefficients, critical organs and the effective dose coefficients to those published in literature. In this thesis the effective dose coefficients for [^{11}C]-labelled compounds were 4.0 μSv/MBq and 4.4 μSv/MBq and for [^{18}F]-labelled compounds 19 μSv/MBq and 18 μSv/MBq, which are typical values to the radiopharmaceuticals labelled with those radionuclides. The effective dose coefficient is higher for [^{18}F] because of the longer physical half-life compared to [^{11}C].

The excretion into urine is specific to certain radiopharmaceuticals and the variation is considerable. The amount of excretion and the time schedule for urinating has an influence on absorbed dose to the urinary bladder wall and the effective dose. The radiation exposure can be reduced with careful planning of urinary bladder voiding times.

At our centre, a protocol for dose evaluation on human subjects, approved by a local ethical committee, is established. In the protocol, a dynamic whole-body scan is performed for six subjects and the dose coefficient is evaluated before a clinical trial is started.

7 Conclusions

In this thesis, radiation exposure and dose coefficients for four different radiopharmaceuticals were studied. Data collection methods were designed for state-of-art PET or PET/CT scanners at the time of each study. Software code used by multiple users was employed for absorbed dose coefficient calculations. The development of PET scanning and changes in calculation software and adjustment of dosimetry models were reported. Effective dose coefficients were convergent to previous published radiation dose estimates and all radiopharmaceuticals used in this research are suitable for clinical use in PET. The dosimetry results in our publications are useful for judging the risks of clinical application and for planning the dosing of these new radiopharmaceuticals.

The findings of each study were as follows:

Study I. The effective dose coefficient of [^{18}F]FETNIM (0.019 mSv/MBq) with the 4-hour urinary bladder voiding period is well within the range of effective dose coefficients of [^{18}F]-labelled radiopharmaceuticals. The absorbed dose to urinary bladder wall can be reduced by increasing the urine excretion rate with frequent bladder voiding after injection. This also reduces the effective dose to the participants and the radiation exposure is lower.

Study II. The effective dose coefficient of [^{11}C]MeAIB (0.004 mSv/MBq) is well within the range of effective dose coefficients of [^{11}C]-labelled radiopharmaceuticals. The absorbed dose coefficient is highest in the pancreas, kidneys, small intestine, liver, and in salivary glands. It is possible to estimate radiation exposure to salivary glands with the spherical phantoms in OLINDA/EXM. The radiation exposure from [^{11}C]MeAIB administration is moderate and the results of this study help the ethical committee to assess the justification for PET studies with this radiopharmaceutical.

Study III. The effective dose coefficient of [^{11}C]choline (0.0044 mSv/MBq) is well within the range of effective dose coefficients of [^{11}C]-labelled radiopharmaceuticals. Human radiation exposure estimate based on preclinical *in vivo* measurements is 36 % lower compared to human based measurements, but preclinical distribution measurements with [^{11}C]choline are in accordance with

human PET measurements, except for the pancreas. Comparisons of preclinical study results to clinical results are rare and it is therefore a strength of this study.

Study IV. This study indicate that [^{18}F]-rhPSMA-7.3 is a well-tolerated PET radiopharmaceutical with a favorable radiation exposure. The effective dose coefficient of 0.018 mSv/MBq (the re-calculated value) with 3.5-hour voiding interval is suitable for clinical imaging and well in the range of other [^{18}F]-labelled radiopharmaceuticals. The dynamic series of whole-body PET/CT imaging proved to be an accurate method for dose assessment.

Acknowledgements

I owe my sincerest thanks to Professor Juhani Knuuti, MD, director of Turku PET Centre for the encouraging and inspiring scientific atmosphere at Turku PET Centre. It is important that there is time for scientific research alongside the clinical work, and his direction has enabled this. I also want to express my gratitude to my supervisor Emeritus Professor Heikki Minn, MD, for encouraging me to continue on the dosimetry project started years earlier and write the doctoral thesis based on it. I am thankful for Professor Mika Teräs, PhD, my supervisor, for his guidance and commentary during the writing of my thesis. With great pleasure I thank Mika for many years of collaboration. He was my mentor for PET physics and instrumentation.

I owe my greatest gratitude to Docent Eero Hippeläinen, PhD, and Docent Mattias Sandström, PhD, for their constrictive comments and critiqeu during the preparation of this thesis. Their work as pre-examinators was excellent. Virpi Tunninen and Jukka Järvinen are acknowledged for forming the follow-up committee for doctoral training.

I am very greatful for all my research team collegues who made these original publications possible. The dosimetry research demanded collaboration from many different experts. The personnel at the Accelerator Laboratory at Åbo Academi and personnel at Radiochemistry Laboratory at Turku University are acknowledged for producing the radiopharmaceuticals. Medical doctors at Turku University Hospital and Professor Anne Roivainen, PhD, are acknowledged for recruiting, studying and acquiring the subjects for dosimetry research in Turku PET Centre. Researchers at Preclinical Laboratory are acknowledged for gathering preclinical data.

I am deeply grateful to the radiographers, medical laboratory technologists and study nurses in Turku PET Centre for their skillful assistance and cooperation. I express my sincere thanks to Vesa Oikonen for guiding me to model and fit the urinary samples data suitable for dosimetry software calculations. Kaisa Lehtiö, Eija Sutinen, Kari Kalliokoski and Tove Grönroos are acknowledged for assistance during the data analysis and writing process.

With great pleasure I thank my colleagues Virva Saunavaara, Reetta Siekkinen, Jukka Ihalainen, Jarmo Teuho, Riku Klén, Sami Suilamo and Tommi Noponen for a

friendly and stimulating work atmosphere and all the support I have received during the doctoral thesis project. IT-team, Marko Tättäläinen, Rami Mikkola and Jani Lehtilä are acknowledged for assisting with computers and softwares.

I want to collectively thank all my friends and friends of my family for fruitful discussions beyond science. The choir of Kaarina church and the cantor Terttu Jussila, the choir conductor, are acknowledged for keeping my mind focused on beautiful music during our rehearsals and performances.

I express my greatest gratitude to my parents Sirkka-Liisa and Kyösti Tolvanen. They have supported my interest towards natural sciences since my childhood and encouraged me to study as long as possible. My sister Terhi Tolvanen with her family and my brother Jarmo Tolvanen with his family are acknowledged for being ready to discuss and share thoughts with me anytime.

I am deeply grateful to my dear husband Esa Eronen, who has kindly balanced my excited periods during the thesis writing process. Your knowledge on physics and dosimetry has been a great help for me. My dear children Mika Niskanen, Ville Niskanen and Kaisa Eronen have brought lots of joy, love, and happiness into my life. Ville is acknowledged for editing English in this thesis.

Finally, I owe my deepest gratitude to all the subjects, who volunteered to participate in this study.

This study was financially supported by the Finnish Cancer Foundation, the Southwestern Finnish Cancer Foundation, the Turku University Foundation, the Academy of Finland (no. 119048), the Hospital District of Southwest Finland (no. EVO13856), and the Blue Earth Diagnostics Ltd.

June 2023
Tuula Tolvanen

References

<*https://doseinfo-radar.com*>.

<*https://WWW.ICRP.org*>.

Afshar-Oromieh, A., Hetzheim, H., Kratochwil, C., Benesova, M., Eder, M., Neels, O. C., Eisenhut, M., Kübler, W., Holland-Letz, T., Giesel, F. L., Mier, W., Kopka, K., & Haberkorn, U. (2015). The theranostic PSMA ligand PSMA-617 in the diagnosis of prostate cancer by PET/CT: Biodistribution in humans, radiation dosimetry, and first evaluation of tumor lesions. *Journal of Nuclear Medicine*, *56*(11), 1697–1705. https://doi.org/10.2967/jnumed.115.161299

Barthel, H., Wilson, H., Collingridge, D. R., Brown, G., Osman, S., Luthra, S. K., Brady, F., Workman, P., Price, P. M., & Aboagye, E. O. (2004). In vivo evaluation of [18F]fluoroetanidazole as a new marker for imaging tumour hypoxia with positron emission tomography. *British Journal of Cancer*, *90*(11). https://doi.org/10.1038/sj.bjc.6601862

Bolch, W. E., Eckerman, K. F., Sgouros, G., Thomas, S. R., Brill, A. B., Fisher, D. R., Howell, R. W., Meredith, R., & Wessels, B. W. (2009). MIRD pamphlet No. 21: A generalized schema for radiopharmaceutical dosimetry-standardization of nomenclature. *Journal of Nuclear Medicine*, *50*(3), 477–484. https://doi.org/10.2967/jnumed.108.056036

Bresser, P. L., Vorster, M., & Sathekge, M. M. (2021). An overview of the developments and potential applications of 68Ga-labelled PET/CT hypoxia imaging. In *Annals of Nuclear Medicine* (Vol. 35, Issue 2, pp. 148–158). Springer Japan. https://doi.org/10.1007/s12149-020-01563-7

Bruce-Chwatt, L. J. (1965). Declaration of Helsinki. Recommendations Guiding Doctors in Clinical Research. *WHO Chronicle*, *19*(June), 31–32. https://doi.org/10.5694/j.1326-5377.1973.tb76647.x

Carter, L. M., Choi, C., Krebs, S., Beattie, B. J., Kim, C. H., Schoder, H., Bolch, W. E., & Kesner, A. L. (2021). Patient Size-Dependent Dosimetry Methodology Applied to 18 F-FDG Using New ICRP Mesh Phantoms . *Journal of Nuclear Medicine*, *62*(12), 1805–1814. https://doi.org/10.2967/jnumed.120.256719

Cherry, S. R., & Dahlbom, M. (2004). PET: Physics, Instrumentation, and Scanners. In *PET* (pp. 1–124). Springer New York. https://doi.org/10.1007/978-0-387-22529-6_1

Cho, S. Y., Gage, K. L., Mease, R. C., Senthamizhchelvan, S., Holt, D. P., Jeffrey-Kwanisai, A., Endres, C. J., Dannals, R. F., Sgouros, G., Lodge, M., Eisenberger, M. A., Rodriguez, R., Carducci, M. A., Rojas, C., Slusher, B. S., Kozikowski, A. P., & Pomper, M. G. (2012). Biodistribution, tumor detection, and radiation dosimetry of 18F-DCFBC, a low-molecular-weight inhibitor of prostate-specific membrane antigen, in patients with metastatic prostate cancer. *Journal of Nuclear Medicine*, *53*(12), 1883–1891. https://doi.org/10.2967/jnumed.112.104661

Christensen, H. N. (1990). Role of amino acid transport and countertransport in nutrition and metabolism. *Physiological Reviews*, *70*(1), 43–77. https://doi.org/10.1152/physrev.1990.70.1.43

Degrado, T. R., Reiman, R. E., David, ;, Price, T., Wang, S., & Coleman, R. E. (2002). Pharmacokinetics and Radiation Dosimetry of 18 F-Fluorocholine. *J Nucl Med*, *42*, 92–96.

Deloar, H. M., Fujiwara, T., Nakamura, T., Itoh, M., Imai, D., Miyake, M., & Watanuki, S. (1998). Estimation of internal absorbed dose of L-[methyl-11 C]methionine using whole-body positron emission tomography. *European Journal of Nuclear Medicine*, *25*(6), 629–633.

Demirci, E., Toklu, T., Yeyin, N., Ocak, M., Alan-Selcuk, N., Araman, A., & Kabasakal, L. (2018). ESTIMATION of the ORGAN ABSORBED DOSES and EFFECTIVE DOSE from 68 Ga-PSMA-11 PET SCAN. *Radiation Protection Dosimetry*, *182*(4), 518–524. https://doi.org/10.1093/rpd/ncy111

Doss, M., Zhang, J. J., Bélanger, M. J., Stubbs, J. B., Hostetler, E. D., Alpaugh, K., Kolb, H. C., & Yu, J. Q. (2010). Biodistribution and radiation dosimetry of the hypoxia marker 18F-HX4 in monkeys and humans determined by using whole-body PET/CT. *Nuclear Medicine Communications*, *31*(12), 1016–1024. https://doi.org/10.1097/MNM.0b013e3283407950

Evans, S. M., Kachur, A. V., Shiue, C. Y., Hustinx, R., Jenkins, W. T., Shive, G. G., Karp, J. S., Alavi, A., Lord, E. M., Dolbier, W. R., & Koch, C. J. (2000). Noninvasive detection of tumor hypoxia using the 2-nitroimidazole [18F]EF1. *Journal of Nuclear Medicine*, *41*(2), 327–336.

Fabbri, C., Galassi, R., Moretti, A., Sintuzzi, E., Mautone, V., Sarti, G., Strigari, L., Benassi, M., & Matteucci, F. (2014). Radiation dosimetry of 18F-flurocholine PET/CT studies in prostate cancer patients. *Physica Medica*, *30*(3), 346–351. https://doi.org/10.1016/j.ejmp.2013.10.007

Ghosh, A., & Heston, W. D. W. (2004). Tumor target prostate specific membrane antigen (PSMA) and its regulation in prostate cancer. *Journal of Cellular Biochemistry*, *91*(3), 528–539. https://doi.org/10.1002/jcb.10661

Giesel, F. L., Hadaschik, B., Cardinale, J., Radtke, J., Vinsensia, M., Lehnert, W., Kesch, C., Tolstov, Y., Singer, S., Grabe, N., Duensing, S., Schäfer, M., Neels, O. C., Mier, W., Haberkorn, U., Kopka, K., & Kratochwil, C. (2017). F-18 labelled PSMA-1007: biodistribution, radiation dosimetry and histopathological validation of tumor lesions in prostate cancer patients. *European Journal of Nuclear Medicine and Molecular Imaging*, *44*(4), 678–688. https://doi.org/10.1007/s00259-016-3573-4

Giussani, A., Janzen, T., Uusijärvi-Lizana, H., Tavola, F., Zankl, M., Sydoff, M., Bjartell, A., Leide-Svegborn, S., Söderberg, M., Mattsson, S., Hoeschen, C., & Cantone, M. C. (2012). A compartmental model for biokinetics and dosimetry of 18F- choline in prostate cancer patients. *Journal of Nuclear Medicine*, *53*(6), 985–993. https://doi.org/10.2967/jnumed.111.099408

Graham, M. M., Peterson, L., Link, J., Evans, M., Rasey, J., Koh, W.-J., Caldwell, J., & Krohn, K. (1997). Fluorine-18-Fluoromisonidazole Radiation Dosimetry in Imaging Studies. *J Nucl Med*, *38*, 1634–1638.

Grönroos, T., Eskola, O., Lehtiö, K., Minn, H., Marjamäki, P., Bergman, J., Haaparanta, M., Forsback, S., & Solin, O. (2001). Pharmacokinetics of [18F]FETNIM: A potential hypoxia marker for PET. *Journal of Nuclear Medicine*, *42*(9), 1397–1404.

Herrmann, K., Bluemel, C., Weineisen, M., Schottelius, M., Wester, H. J., Czernin, J., Eberlein, U., Beykan, S., Lapa, C., Riedmiller, H., Krebs, M., Kropf, S., Schirbel, A., Buck, A. K., & Lassmann, M. (2015). Biodistribution and radiation dosimetry for a probe targeting prostate-specific membrane antigen for imaging and therapy. *Journal of Nuclear Medicine*, *56*(6), 855–861. https://doi.org/10.2967/jnumed.115.156133

Hohberg, M., Kobe, C., Krapf, P., Täger, P., Hammes, J., Dietlein, F., Zlatopolskiy, B. D., Endepols, H., Wild, M., Neubauer, S., Heidenreich, A., Neumaier, B., Drzezga, A., & Dietlein, M. (2019). Biodistribution and radiation dosimetry of [18F]-JK-PSMA-7 as a novel prostate-specific membrane antigen-specific ligand for PET/CT imaging of prostate cancer. *EJNMMI Research*, *9*(1). https://doi.org/10.1186/s13550-019-0540-7

Howell, R. W., Wessels, B. W., Loevinger, R., Watson, E., Bolch, W. E., Brill, A. B., Charkes, N. D., Fisher, D. R., Hays, M. T., Robertson, J. S., Siegel, J. A., Thomas, S. R., & Wessels, B. W. (1999). The MIRD Perspective 1999. *J Nucl Med*, *40*, 3S-10S.

Huang, Y., Fan, J., Li, Y., Fu, S., Chen, Y., & Wu, J. (2021). Imaging of Tumor Hypoxia With Radionuclide-Labeled Tracers for PET. In *Frontiers in Oncology* (Vol. 11). Frontiers Media S.A. https://doi.org/10.3389/fonc.2021.731503

ICRP. (1979). Limits for Intakes of Radionuclides by Workers ICRP Publication 30. *Annals of the ICRP*, *2*(3/4).

ICRP. (1981). Annals of the ICRP. *Annals of the ICRP*, *6*(1), 1. https://doi.org/10.1016/0146-6453(81)90127-5

ICRP. (1987a). Protection of the Patient in Nuclear Medicine (and Statement from the 1987 Como Meeting of ICRP). ICRP Publication 52. *Annals of the ICRP*, *17*(4).

ICRP. (1987b). Radiation Dose to Patients from Radiopharmaceuticals ICRP Publication 53. *Annals of the ICRP*, *18*(1–4).

ICRP. (1991a). 1990 Recommendations of the ICRP. *Annals of the ICRP*, *21*(1–3), 67–77.

ICRP. (1991b). Biological Protection in Biomedicine Research ICRP Publication 62. *Annals of the ICRP*, *22*.

ICRP. (1998). Radiation dose to patients from radiopharmaceuticals (Addendum 2 to ICRP publication 53) ICRP publication 80 approved by the Commission in September 1997. *Annals of the ICRP*, *28*(3). https://doi.org/10.1016/S0146-6453(99)00006-8

ICRP. (2003). Relative Biological Effectiveness (RBE), Quality Factor (Q), and Radiation weighting Factor (wR) ICRP Publication 92. *Annals of the ICRP*.

ICRP. (2008). Radiation dose to patients from radiopharmaceuticals. Addendum 3 to ICRP Publication 53. ICRP Publication 106. Approved by the Commission in October 2007. *Annals of the ICRP*, *38*(1–2).

ICRP. (2015). ICRP Publication 128: Radiation Dose to Patients from Radiopharmaceuticals: A Compendium of Current Information Related to Frequently Used Substances. *Annals of the ICRP*, *44*(2_suppl). https://doi.org/10.1177/0146645314558019

Jacobson, O., Kiesewetter, D. O., & Chen, X. (2015). Fluorine-18 radiochemistry, labeling strategies and synthetic routes. *Bioconjugate Chemistry*, *26*(1), 1–18. https://doi.org/10.1021/bc500475e

Johansson, L., Mattsson, S., Nosslin, B., & Leide-Svegborn, S. (1992). Effective dose from radiopharmaceuticals. *European Journal of Nuclear Medicine*, *19*(11). https://doi.org/10.1007/BF00175858

Josefsson, A., Siritantikorn, K., Ranka, S., de Amorim de Carvalho, J. W., Buchpiguel, C. A., Sapienza, M. T., Bolch, W. E., & Sgouros, G. (2020). Accuracy in dosimetry of diagnostic agents: impact of the number of source tissues used in whole organ S value-based calculations. *EJNMMI Research*, *10*(1). https://doi.org/10.1186/s13550-020-0614-6

Katz-Brull, R., & Degani, H. (1996). Kinetics of choline transport and phosphorylation in human breast cancer cells; NMR application of the zero trans method. *Anticancer Research*, *16 3B*, 1375–1380.

Kim, J. Y., Park, H., Lee, J. C., Kim, K. M., Lee, K. C., Ha, H. J., Choi, T. H., An, G. Il, & Cheon, G. J. (2009). A simple Cu-64 production and its application of Cu-64 ATSM. *Applied Radiation and Isotopes*, *67*(7–8), 1190–1194. https://doi.org/10.1016/j.apradiso.2009.02.060

Kirschner, A., Ice, R., & Beierwaltes, W. (1975). Radiation Dosimetry of 131I-19-Iodocholesterol: The Pitfalls of Using Tissue Concentration Data-Reply. *Journal of Nuclear Medicine*, *16*(3), 248–249.

Knorr, K., Oh, S. W., Krönke, M., Wurzer, A., D'Alessandria, C., Herz, M., Weber, W., Wester, H. J., Eiber, M., Yusufi, N., & Nekolla, S. (2022). Preclinical biodistribution and dosimetry and human biodistribution comparing 18F-rhPSMA-7 and single isomer 18F-rhPSMA-7.3. *EJNMMI Research*, *12*(1). https://doi.org/10.1186/s13550-021-00872-w

Laforest, R., Dehdashti, F., Lewis, J. S., & Schwarz, S. W. (2005). Dosimetry of 60/61/62/64Cu-ATSM: A hypoxia imaging agent for PET. *European Journal of Nuclear Medicine and Molecular Imaging*, *32*(7), 764–770. https://doi.org/10.1007/s00259-004-1756-x

Lin, L. L., Silvoniemi, A., Stubbs, J. B., Rengan, R., Suilamo, S., Solin, O., Divgi, C., Eskola, O., Sorger, J. M., Stabin, M. G., Kachur, A., Hahn, S. M., Grönroos, T. J., Forsback, S., Evans, S. M., Koch, C. J., & Minn, H. (2012). Radiation dosimetry and biodistribution of the hypoxia tracer 18F-EF5 in oncologic patients. *Cancer Biotherapy and Radiopharmaceuticals*, *27*(7), 412–419. https://doi.org/10.1089/cbr.2011.1130

Liu, T., Liu, C., Zhang, Z., Zhang, N., Guo, X., Xia, L., Jiang, J., Xie, Q., Yan, K., Rowe, S. P., Zhu, H., & Yang, Z. (2021). 64Cu-PSMA-BCH: a new radiotracer for delayed PET imaging of prostate

cancer. *European Journal of Nuclear Medicine and Molecular Imaging*, *48*(13), 4508–4516. https://doi.org/10.1007/s00259-021-05426-9

Loevinger, R., Budinger, T., & Watson, E. (1988). *MIRD Primer for Absorbed Dose Calculations*.

Mahy, P., Geets, X., Lonneux, M., Levêque, P., Christian, N., De Bast, M., Gillart, J., Labar, D., Lee, J., & Grégoire, V. (2008). Determination of tumour hypoxia with [18F]EF3 in patients with head and neck tumours: A phase I study to assess the tracer pharmacokinetics, biodistribution and metabolism. *European Journal of Nuclear Medicine and Molecular Imaging*, *35*(7), 1282–1289. https://doi.org/10.1007/s00259-008-0742-0

Någren, K., Sutinen, E., & Jyrkkiö, S. (2000). [N-methyl-11C]MeAIB, a Tracer for System A Amino Acid Transport: Preparation from [11C]Methyk Triflate an HPLC Metabolite Analysis of Plasma Samples After Intravenous Administration in Man. *Journal of Labelled Compounds and Radiopharmaceuticals*, *43*, 1013–1021.

Nario, A. P., Woodfield, J., dos Santos, S. N., Bergman, C., Wuest, M., Araújo, Y. B., Lapolli, A. L., West, F. G., Wuest, F., & Bernardes, E. S. (2022). Synthesis of a 2-nitroimidazole derivative N-(4-[18F]fluorobenzyl)-2-(2-nitro-1H-imidazol-1-yl)-acetamide ([18 F]FBNA) as PET radiotracer for imaging tumor hypoxia. *EJNMMI Radiopharmacy and Chemistry*, *7*(1). https://doi.org/10.1186/s41181-022-00165-0

Nosske, D., & Brix, G. (2009). Dose assessment for C-11- and F-18-choline. In *J Nucl Med Med: Vol. 50 (supp.2*.

Patton, J. A. (2002). Physics of PET. In *Practical FDG Imaging: A Teaching File* (pp. 18–36). Springer New York. https://doi.org/10.1007/978-0-387-22453-4_2

Pfob, C. H., Ziegler, S., Graner, F. P., Köhner, M., Schachoff, S., Blechert, B., Wester, H. J., Scheidhauer, K., Schwaiger, M., Maurer, T., & Eiber, M. (2016). Biodistribution and radiation dosimetry of 68Ga-PSMA HBED CC—a PSMA specific probe for PET imaging of prostate cancer. *European Journal of Nuclear Medicine and Molecular Imaging*, *43*(11), 1962–1970. https://doi.org/10.1007/s00259-016-3424-3

Piron, S., De Man, K., Van Laeken, N., D'Asseler, Y., Bacher, K., Kersemans, K., Ost, P., Decaestecker, K., Deseyne, P., Fonteyne, V., Lumen, N., Achten, E., Brans, B., & De Vos, F. (2019). Radiation dosimetry and biodistribution of 18F-PSMA-11 for PET imaging of prostate cancer. *Journal of Nuclear Medicine*, *60*(12), 1736–1742. https://doi.org/10.2967/jnumed.118.225250

Plyku, D., Mena, E., Rowe, S. P., Lodge, M. A., Szabo, Z., Cho, S. Y., Pomper, M. G., Sgouros, G., & Hobbs, R. F. (2018). Combined model-based and patient-specific dosimetry for 18F-DCFPyL, a PSMA-targeted PET agent. *European Journal of Nuclear Medicine and Molecular Imaging*, *45*(6), 989–998. https://doi.org/10.1007/s00259-018-3939-x

Ramírez de Molina, A., Rodríguez-González, A., Gutiérrez, R., Martínez-Piñeiro, L., Sánchez, J. J., Bonilla, F., Rosell, R., & Lacal, J. C. (2002). Overexpression of choline kinase is a frequent feature in human tumor-derived cell lines and in lung, prostate, and colorectal human cancers. *Biochemical and Biophysical Research Communications*, *296*(3), 580–583. https://doi.org/https://doi.org/10.1016/S0006-291X(02)00920-8

Reischl, G., Dorow, D., Cullinane, C., Katsifis, A., Roselt, P., Binns, D., & Hicks, R. (2007). Imaging of tumor hypoxia with [124I]IAZA in comparison with [18F]FMISO and [18F]FAZA-firsto small animal PET results. *J Pharm Pharm Sci*, *10*, 203–211.

Roivainen, A., Forsback, S., Grönroos, T., Lehikoinen, P., Kähkönen, M., Sutinen, E., & Minn, H. (2000). Blood Metabolism of [methyl-11C]-choline; implications for in vivo imaging with positron emission tomography. *Eur j Nucl Med*, *27*, 25–32.

Savi, A., Incerti, E., Fallanca, F., BettinarDi, V., Rossetti, F., Monterisi, C., Compierchio, A., Negri, G., Zannini, P., Gianolli, L., & Picchio, M. (2017). First evaluation of PET-based human bioDistribution and dosimetry of 18F-FAZA, a tracer for imaging tumor hypoxia. *Journal of Nuclear Medicine*, *58*(8), 1224–1229. https://doi.org/10.2967/jnumed.113.122671

Siegel, J. A., Thomas, S. R., Stubbs, J. B., Stabin, M. G., Hays, M. T., Koral, K. F., Robertson, J. S., Howell, R. W., Wessels, B. W., Fisher, D. R., Weber, D. A., & Brill, A. B. (1999). MIRD pamphlet no. 16: Techniques for quantitative radiopharmaceutical biodistribution data acquisition and analysis for use in human radiation dose estimates. *Journal of Nuclear Medicine*, *40*(2), 37–61.

Silver, A., & Fair, R. (1997). *Prostate-specific and*. *3*(January), 81–85.

Society of Nuclear Medicine and Molecular Imaging. *Committee on Medical Internal Radiation Dose (MIRD) - SNMMI*. http://www.snmmi.org/AboutSNMMI/CommitteeContent.aspx?ItemNumber=12475&navItemNumber=763 (Accessed 4th March 2022)

Stabin, M. G. (1996). MIRDOSE:Personal Computer Software for Internal Dose Assessment in Nuclear Medicine. *J Nucl Med*, *37*, 538–546.

Stabin, M. G. (2008). Uncertainties in internal dose calculations for radiopharmaceuticals. *Journal of Nuclear Medicine*, *49*(5), 853–860. https://doi.org/10.2967/jnumed.107.048132

Stabin, M. G. (2017). Radiation Dosimetry of PET Imaging. In M. M. Khalil (Ed.), *Basic Science of PET Imaging* (pp. 65–76). Springer International Publishing. https://doi.org/10.1007/978-3-319-40070-9_3

Stabin, M. G., Sparks, R. B., & Crowe, E. (2005). OLINDA/EXM: The Second-Generation Personal Computer Software for Internal Dose Assessment in Nuclear Medicine. *J Nucl Med*, *46*, 1023–1027.

Tolvanen, T., Kalliokoski, K., Malaspina, S., Kuisma, A., Lahdenpohja, S., Postema, E. J., Miller, M. P., & Scheinin, M. (2021). Safety, Biodistribution, and Radiation Dosimetry of 18F-rhPSMA-7.3 in Healthy Adult Volunteers. *Journal of Nuclear Medicine*, *62*(5), 679–684. https://doi.org/10.2967/jnumed.120.252114

Tolvanen, T., Lehtiö, K., Kulmala, J., Oikonen, V., Eskola, O., Bergman, J., & Minn, H. (2002). 18F-fluoroerythronitroimidazole radiation dosimetry in cancer studies. *Journal of Nuclear Medicine*, *43*(12).

Tolvanen, T., Någren, K., Yu, M., Sutinen, E., Havu-Aurén, K., Jyrkkiö, S., Asola, M., Kotoneva, E., Nuutila, P., & Minn, H. (2006). Human radiation dosimetry of [11C]MeAIB, a new tracer for imaging of system A amino acid transport. *European Journal of Nuclear Medicine and Molecular Imaging*, *33*(10), 1178–1184. https://doi.org/10.1007/s00259-006-0096-4

Tolvanen, T., Yli-Kerttula, T., Ujula, T., Autio, A., Lehikoinen, P., Minn, H., & Roivainen, A. (2010). Biodistribution and radiation dosimetry of [11C]choline: A comparison between rat and human data. *European Journal of Nuclear Medicine and Molecular Imaging*, *37*(5), 874–883. https://doi.org/10.1007/s00259-009-1346-z

Tu, Z., & Mach, R. H. (2010). C-11 Radiochemistry in Cancer Imaging Applications. *Current Topics in Medicinal Chemistry*, *10*(11), 1060–1095. https://doi.org/10.2174/156802610791384261

Wambersie. (2002). THE INTERNATIONAL COMMISSION ON RADIATION UNITS AND MEASUREMENTS. *Journal of the ICRU*, *2*, 1–4.

Watanabe, S., Shiga, T., Hirata, K., Magota, K., Okamoto, S., Toyonaga, T., Higashikawa, K., Yasui, H., Kobayashi, J., Nishijima, K. ichi, Iseki, K., Matsumoto, H., Kuge, Y., & Tamaki, N. (2019). Biodistribution and radiation dosimetry of the novel hypoxia PET probe [18F]DiFA and comparison with [18F]FMISO. *EJNMMI Research*, *9*(1). https://doi.org/10.1186/s13550-019-0525-6

Weber, M. J., Evans, P. K., Johnson, M. A. T., McNair, T., Nakamura, K. D., & Salter, D. W. (1984). Transport of potassium, amino acids, and glucose in cells transformed by Rous sarcoma virus. *Federation Proceedings*, *43 1*, 107–112.

Wibmer, A., Burger, I., Sala, E., Hricak, H., Weber, W., & Vargas, H. (2016). Molecular Imaging of Prostate Cancer. *Radiographics*, *36*, 142–159.

Wurzer, A., Di Carlo, D., Herz, M., Richter, A., Robu, S., Schirrmacher, R., Mascarin, A., Weber, W., Eiber, M., Schwaiger, M., & Wester, H.-J. (2021). Automated synthesis of [18F]Ga-rhPSMA-7/ -

7.3: results, quality control and experience from more than 200 routine productions. *EJNMMI Radiopharmacy and Chemistry*, *6*(1), 4. https://doi.org/10.1186/s41181-021-00120-5

Yang, D. J., Wallace, S., Cherif, A., Li, C., Gretzer, M. B., Kim, E. E., & Podoloff, D. A. (1995). Development of F-18 - Labeled fluoroerythronitroimidazole as a PET agent for imaging tumor hypoxia. *Radiology*, *194*(3), 795–800. https://doi.org/10.1148/radiology.194.3.7862981

Zeisel, S. (1996). Choline. A nutrient that is involved in the regulation of cell proliferation, cell death, and cell transformation. *Adv Exp Med Biol*, *399*, 131–141.

Zhang, J., Lin, Z., Zhang, X., Lin, R., Cui, M., Miao, W., & Yao, S. (2022). 68Ga-DOTA-DiPSMA PET/CT Imaging: Biodistribution, Dosimetry, and Preliminary Application in Prostate Cancer. *Frontiers in Bioengineering and Biotechnology*, *9*(January), 1–9. https://doi.org/10.3389/fbioe.2021.811972

TURUN
YLIOPISTO
UNIVERSITY
OF TURKU

Painosalama, Turku, Finland 2023

ISBN 978-951-29-9302-4 (PRINT)
ISBN 978-951-29-9303-1 (PDF)
ISSN 0355-9483 (Print)
ISSN 2343-3213 (Online)